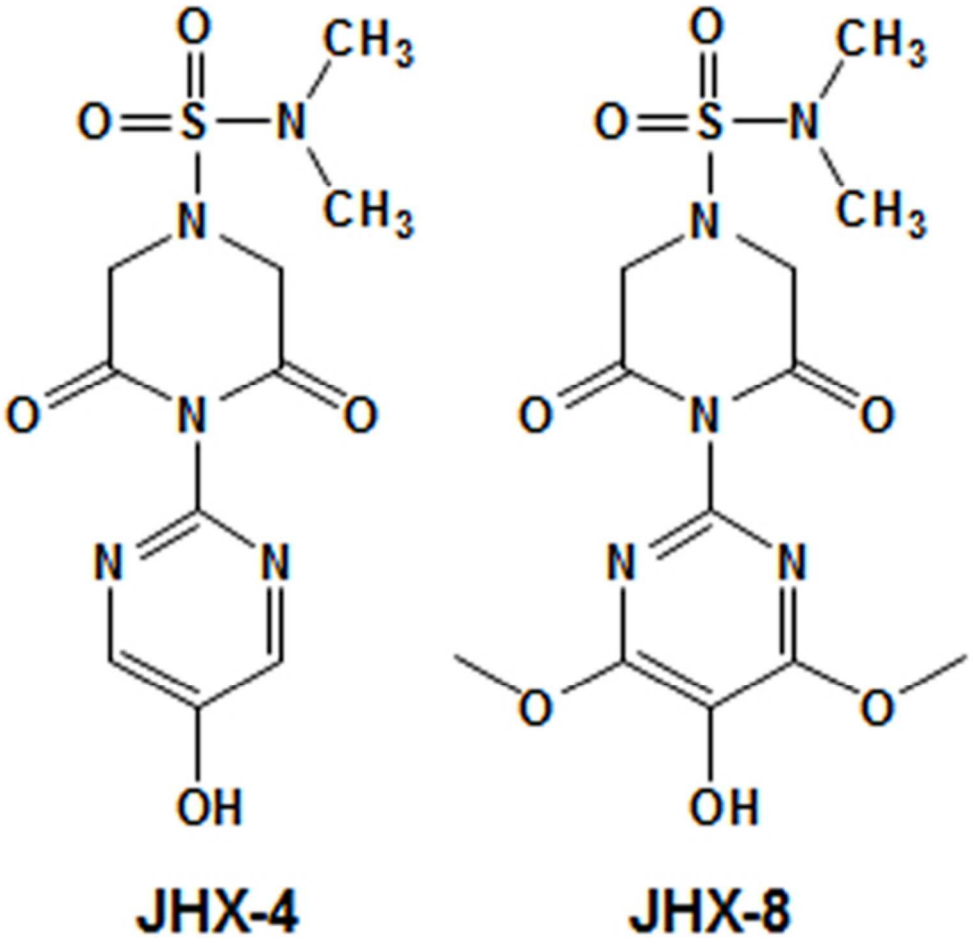

42x42mm (300 x 300 DPI)

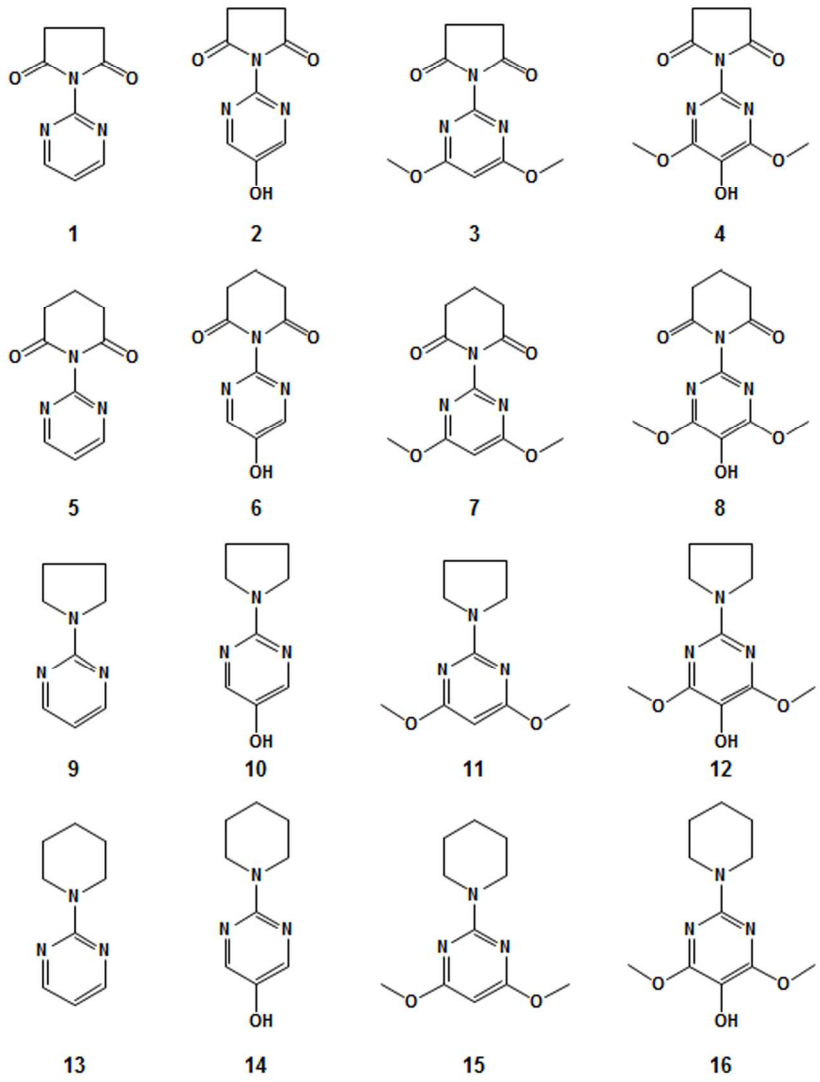

Structures of synthesized compounds in the MFAO-2 series. Shown are multifunctional compounds 2, 4, 6, and 8; mono-functional chelators (CHL), 1, 3, 5, and 7; monofunctional free radical scavengers (FRS), 10, 12, 14, and 16, and the non-functional parent compounds, 9, 11, 13, and 15.
133x190mm (300 x 300 DPI)

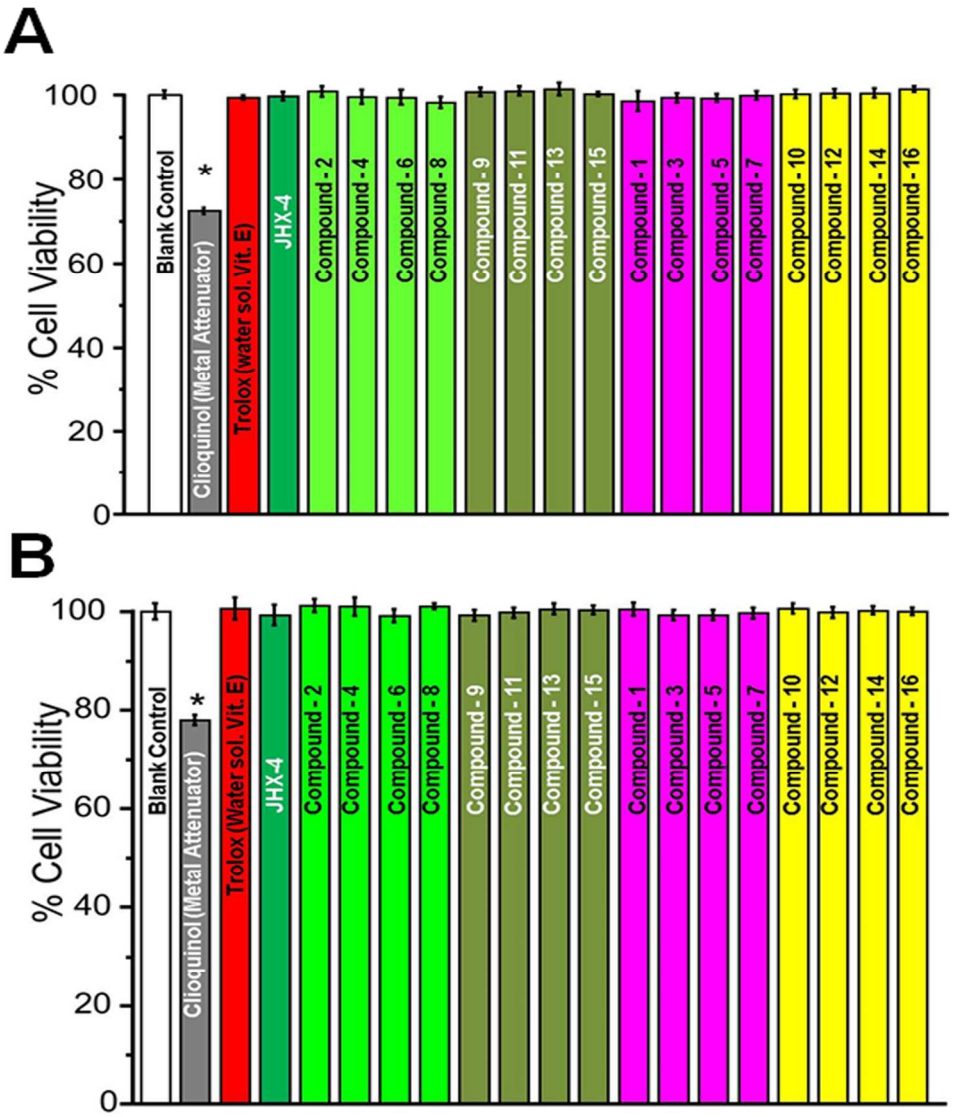

Effect of compound exposure on cell viability of hNBs and RPE cells measured by the MTS viability assay. A illustrates the cell viability of RPEs after 2 h exposure to 1 mM of compounds 1-16, clioquinol, or Trolox. B illustrates the cell viability of hNBs after similar exposure to compounds. The results represent the mean ± SEM, n = 4. Significant differences ($p < 0.05$), calculated by ANOVA, were compared to blank control.
124x149mm (300 x 300 DPI)

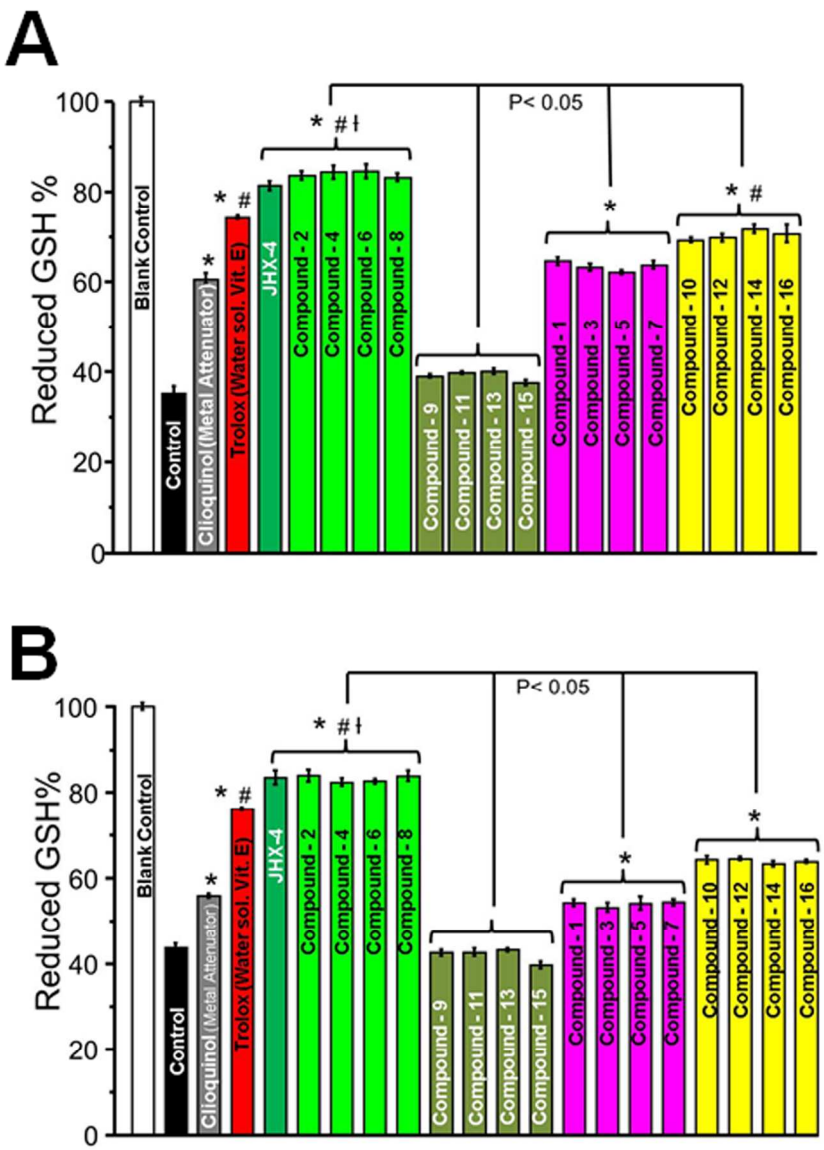

Changes in GSH levels in cells exposed to hydroxyl radicals with/without the presence of compounds 1-16, Trolox, or clioquinol. B illustrates GSH levels of RPEs exposed for 2 h with 1 mM of Fenton reagent with/without the presence of 1 mM of compounds 1-16, clioquinol, or Trolox. B illustrates GSH levels of similarly exposed hNB cells. The results represent the mean ± SEM (n = 6). Significant differences, calculated by ANOVA, were as follows: * $p < 0.05$ versus control, # $p < 0.05$ versus clioquinol, and ł $p < 0.05$ versus Trolox.
127x175mm (300 x 300 DPI)

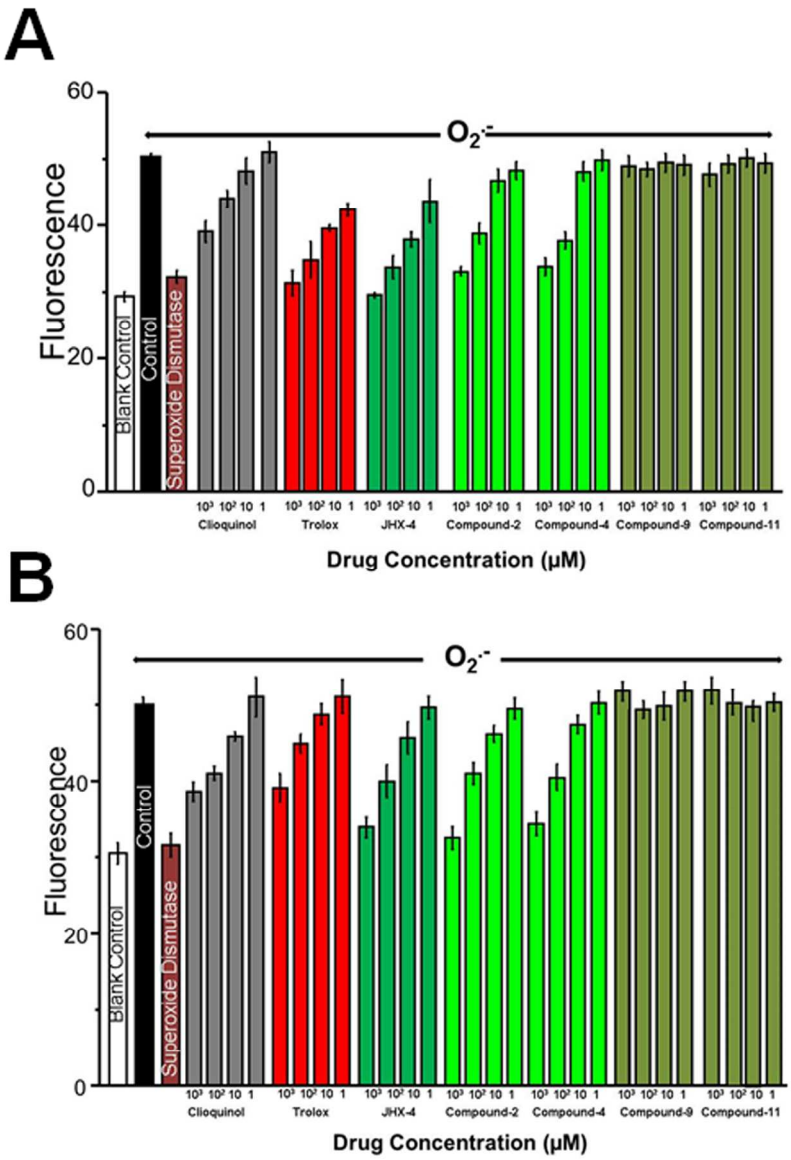

Dose-dependent reduction of superoxide generated by xanthine oxidase and measured by MitoSOX staining in hNB and RPE cells. In A hNBs were pre-incubated with/without the presence of 1, 10, 100, 1000 μM compounds 2, 4, 9, 11, JHX-4, clioquinol or Trolox as well as SOD (25 μg/mL, approximately 100 μM) for 1hr and then exposed to xanthine oxidase (25 mU/mL) which can generate approximately 100 μM of superoxide for 1hr. B illustrates the results of similar experimental procedures of RPEs. The results represents mean ± SEM, n = 6.
135x186mm (300 x 300 DPI)

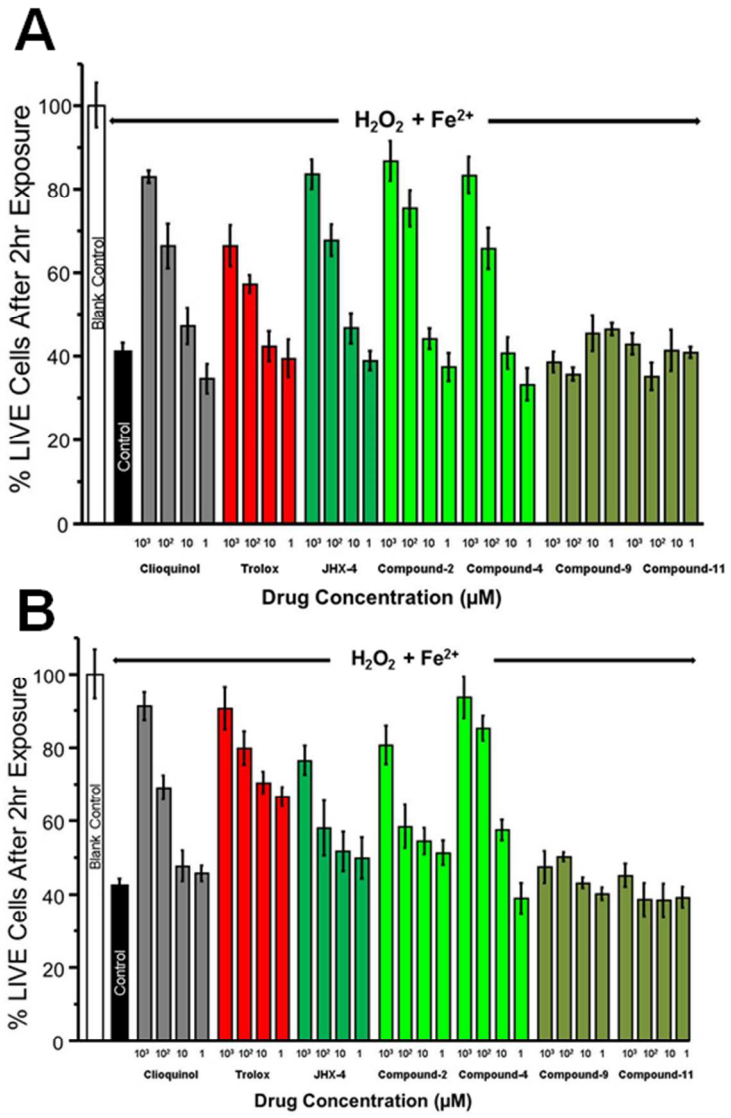

Dose-dependent protection of cells against hydroxyl radicals measured with the LIVE/DEAD Viability Assay. A illustrates the results of hNB cells that were pre-incubated for 1 hr with/without the presence of 1, 10, 100, 1000 μM of compounds 2, 4, 9, 11, JHX-4, clioquinol, or Trolox for 1hr and exposed to 100 μM Fenton reagent for 2hr. B illustrates the results of similar exposure of RPEs as above. The results represents mean ± SEM, n = 6.
52x76mm (300 x 300 DPI)

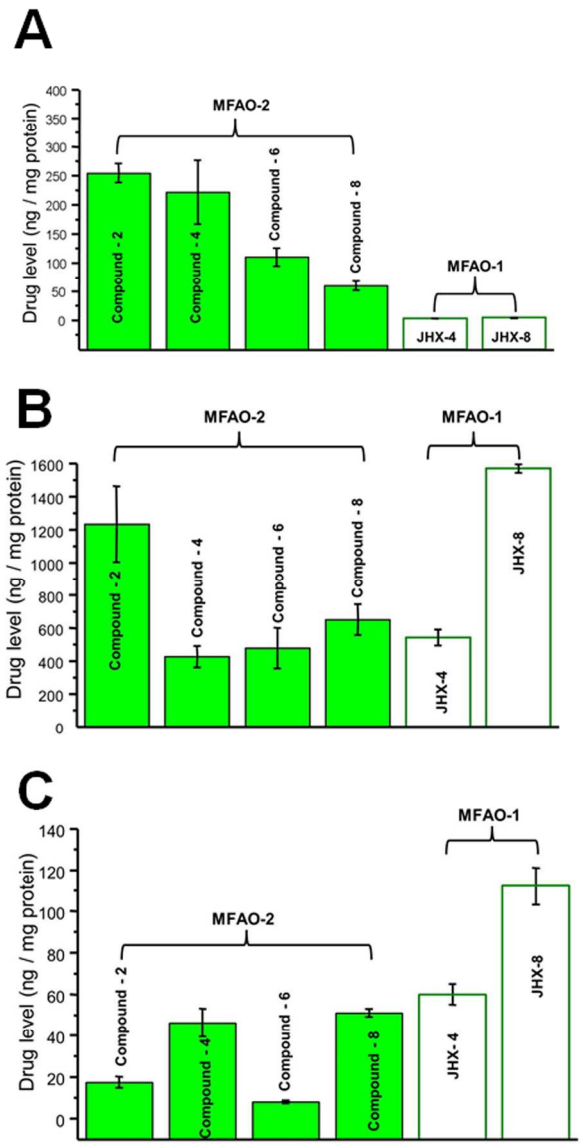

Oral bioavailability of MFAOs in mice. Tissue levels of MFAOs measured in the brain (A), neural retina (B), and lens (C) of C57BL/6 mice fed chow containing 0.05% of each MFAO (80 mg/kg/day average dose) for 14 days. The results represent the mean ± SEM (n = 6-7). The present MFAO-2s achieved higher brain levels compared to the previously synthesized MFAO-1 (A) but failed to reach adequate levels in the lens (C). Similar neural retinal levels were observed with both MFAO-1 and MFAO-2 (B).
129x243mm (300 x 300 DPI)

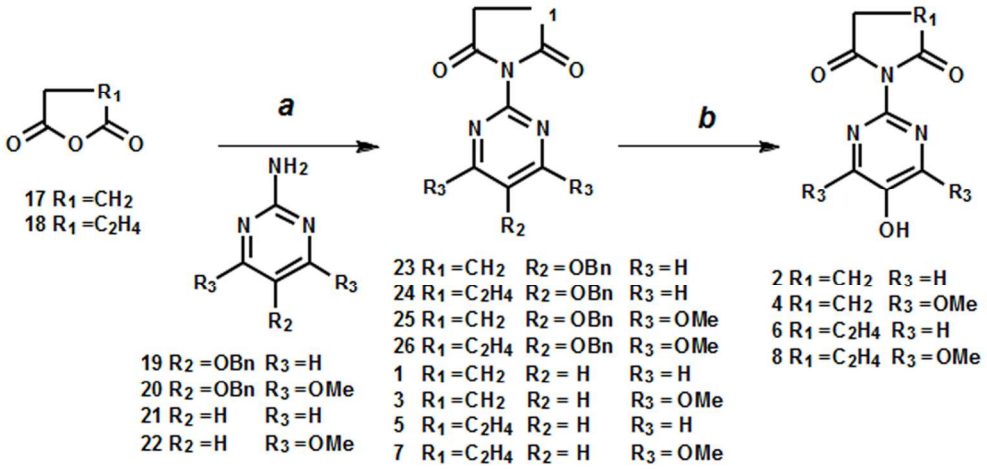

109x52mm (300 x 300 DPI)

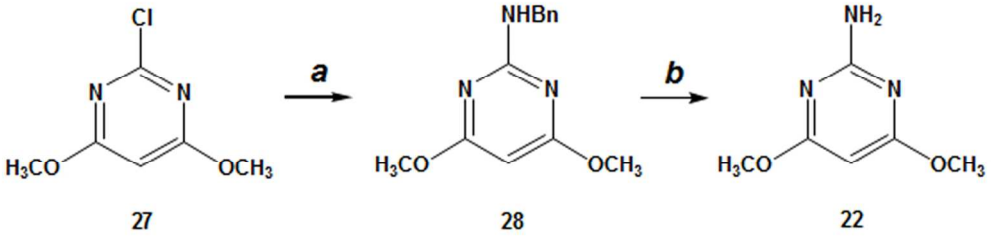

27 28 22

101x25mm (300 x 300 DPI)

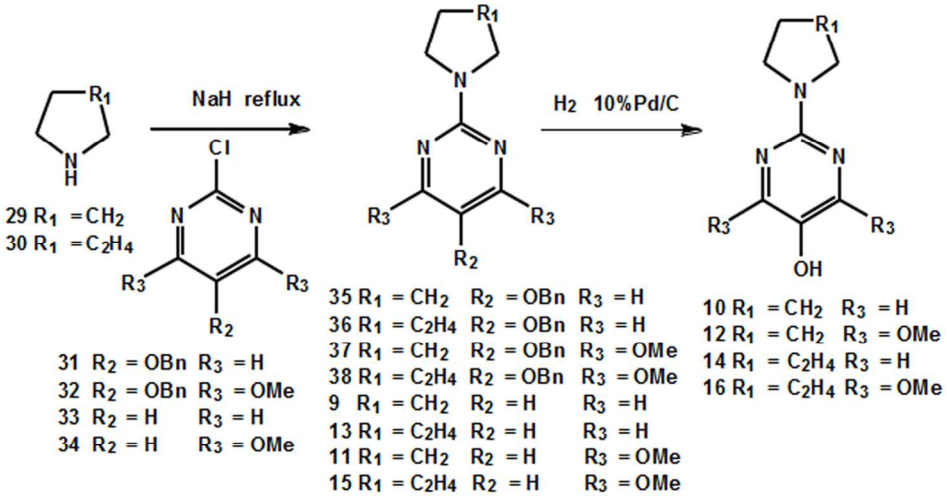

110x66mm (300 x 300 DPI)

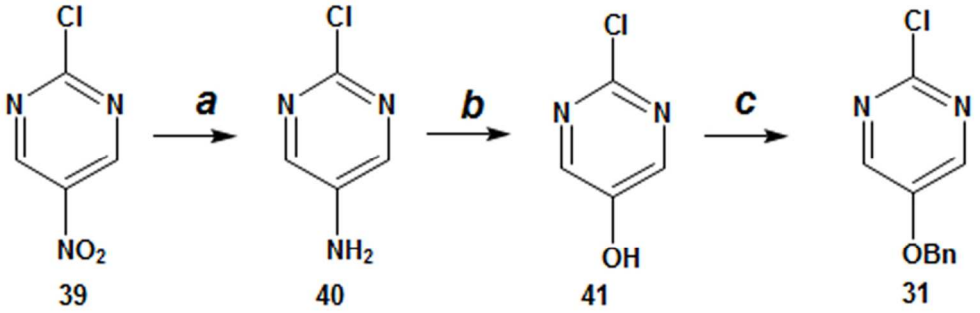

82x29mm (300 x 300 DPI)

Compound	Fe^{2+}	Fe^{3+}	Cu^{+}	Cu^{2+}	Zn^{2+}	Mn^{2+}	Mg^{2+}	Ca^{2+}
1	1.00 : 2.06 ± 0.04	1.00 : 2.01 ± 0.02	1.00 : 2.01 ± 0.17	1.00 : 2.28 ± 0.15	1.00 : 1.87 ± 0.14	1.00 : 1.98 ± 0.07	0*	0*
2	1.00 : 2.06 ± 0.10	1.00 : 2.01 ± 0.05	1.00 : 2.01 ± 0.16	1.00 : 2.28 ± 0.21	1.00 : 1.87 ± 0.14	1.00 : 2.14 ± 0.11	0*	0*
3	1.00 : 2.02 ± 0.08	1.00 : 2.05 ± 0.03	1.00 : 1.92 ± 0.05	1.00 : 2.01 ± 0.16	1.00 : 2.07 ± 0.04	1.00 : 2.04 ± 0.01	0*	0*
4	1.00 : 2.03 ± 0.03	1.00 : 2.12 ± 0.27	1.00 : 2.03 ± 0.14	1.00 : 2.13 ± 0.21	1.00 : 2.01 ± 0.16	1.00 : 2.22 ± 0.05	0*	0*
5	1.00 : 2.13 ± 0.15	1.00 : 1.80 ± 0.03	1.00 : 1.90 ± 0.06	1.00 : 2.01 ± 0.01	1.00 : 2.17 ± 0.08	1.00 : 1.83 ± 0.11	0*	0*
6	1.00 : 1.85 ± 0.07	1.00 : 1.92 ± 0.06	1.00 : 1.86 ± 0.14	1.00 : 1.75 ± 0.05	1.00 : 1.99 ± 0.02	1.00 : 1.91 ± 0.02	0*	0*
7	1.00 : 1.96 ± 0.09	1.00 : 2.08 ± 0.07	1.00 : 1.90 ± 0.03	1.00 : 1.96 ± 0.05	1.00 : 2.06 ± 0.22	1.00 : 1.95 ± 0.24	0*	0*
8	1.00 : 1.97 ± 0.13	1.00 : 1.82 ± 0.05	1.00 : 1.97 ± 0.03	1.00 : 1.86 ± 0.11	1.00 : 2.09 ± 0.13	1.00 : 2.12 ± 0.02	0*	0*

Compound to metal ion ratio of select metal ions. The stoichiometry of the compound to metal complexes was obtained from the intersection of lines in Job's plots. The total concentration of the compound 1-8 and metal ion was 0.1 - 0.5 mM. * Non-intersecting lines on the Job Plot. Mean ± S.D.; n=3
161x73mm (300 x 300 DPI)

Orally Bioavailable Metal Chelators and Radical Scavengers: Multifunctional Antioxidants for the Coadjutant Treatment of Neurodegenerative Diseases

Hiroyoshi Kawada and Peter F. Kador*

Department of Pharmaceutical Sciences, College of Pharmacy, University of Nebraska Medical Center, 986025 Nebraska Medical Center, Omaha, Nebraska 68198-6025, United States of America.

ABSTRACT

Neurodegenerative diseases are associated with oxidative stress that is induced by the presence of reactive oxygen species and the abnormal cellular accumulation of transition metals. Here, a new series of orally bioavailable multifunctional antioxidants (MFAO-2s) possessing a 2-diacetylamino-5-hydroxypyrimidine moiety is described. These MFAO-2s demonstrate both free radical and metal attenuating properties that are similar to the original published MFAO-1s that are based on 1-N, N'-dimethylsulfamoyl-1-4-(2-pyrimidyl)piperazine. Oral bioavailability studies in C57BL/6 mice demonstrate that the MFAO-2s accumulate in the brain at significantly higher levels than the MFAO-1s while achieving similar neural retina levels. The MFAO-2s protect human neuroblastoma and retinal pigmented epithelial cells against hydroxyl radicals in a dose-dependent manner by maintaining cell viability and intracellular glutathione levels. The MFAO-2s outperform clioquinol, a metal attenuator that has been investigated for the treatment of Alzheimer's disease.

INTRODUCTION

Oxidative stress results from an imbalance between oxidants, such as reactive oxygen species (ROS), and antioxidants, such as superoxide dismutase (SOD). An imbalance favoring oxidants can lead to protein, lipid-oxidation, and DNA tissue damage that is associated with age-related cataract, age-related macular degeneration (AMD), and Alzheimer's disease (AD)[1-4]. In addition to oxidative stress, an age-related accumulation of redox-active metals, such as iron and copper, also occurs in the lens, retina, and brain of patients with age related cataracts, AMD and AD[5-8]. When combined with ROS, the increased presence of redox-active metal ions can promote further tissue damage by generating hydroxyl radicals through the Fenton reaction[9]. In AD, ROS is generated by mitochondrial dysfunction, the presence of beta-amyloid peptide (Aβ) and redox metal ions such as Fe^{2+} and Cu^{2+}, and activated glial cells[15]. Increased Mn levels can also contribute to mitochondrial dysfunction as well as impaired energy metabolism, excitotoxic neuronal death, apoptotic death, and oxidation of cellular components[10-13]. Aβ also binds Zn to form neurotoxic plaque that results in localized oxidative stress and neuronal death[14]. Aβ plaque is also present in the retinas of patients with AMD[15, 16] and in the lenses of AD patients with cataracts[17]. The increased presence of Aβ plaque in these age-related diseases is accompanied by the dramatic loss of αB crystallin[18], a zinc binding protein chaperone.

Currently, there is no treatment for preventing the onset, slowing the progression, or reversing these age-related diseases. For AD, approved treatments such as acetylcholinesterase inhibitors (AChEIs) and memantine, an *N*-methyl-D-aspartate

(NMDA) receptor antagonist, only target the symptoms of AD. While these can temporarily improve cognitive and daily function, they do not significantly modify the progression of this disease. The majority of emerging disease-modifying AD treatments target Aβ based on the amyloid hypothesis[19] including reducing Aβ production, increasing Aβ removal from the brain immune-therapeutically, or modulating Aβ toxicity[20]. In addition, an alternative strategy has evolved that links metal dyshomeostasis, i.e., the modulation of metal-protein interactions linked to Aβ and tau neuropathology, to the treatment of AD[21]. In the brain, metal dyshomeostasis of the transition metals copper, zinc and iron have been linked to not only to AD but several other neurodegenerative disorders[22]. For example, the availability of zinc at the glutamatergic synapse is crucially involved in learning and memory and its availability has been shown to decline with age and AD[23]. Copper levels have also been linked to learning and memory[24] and the onset of Huntington's disease (HD) is associated with increased copper-protein interactions in the brain[14, 25]. Iron deposition in the brain (mainly in the Basal Ganglia) has also been linked to cognitive decline and the onset of Parkinson's disease (PD)[26].

Metal dyshomeostasis has been evaluated with the metal attenuators clioquinol (PBT1, 5-chloro-7-iodoquinolin-8-ol), a first generation 8-hydroxyquinoline (8-OHQ) analog, and PBT2 (5,7-dichloro-2-((dimethylamino)methyl) quinolin-8-ol), a second generation 8-OHQ analog, and shown to be effective in animal models of AD, HD and PD[27, 28]. In a Phase IIa clinical trial in AD patients, a 250 mg daily dose of PBT2 has also been shown to be safe, effective in reducing cerebrospinal fluid (CSF) Aβ levels, and improving cognitive performance[29, 30]. A similar dose of PBT2 has been shown to be generally safe

and well-tolerated in patients with HD, where an improvement in a measure of executive function (cognition) was observed[31]. However, the clinical efficacy of PBT2 in both AD and HD studies is controversial[32]. This may be related to the fact that in addition to the metal dyshomeostasis of the transition metals iron, copper or zinc, neurodegenerative diseases are also linked to oxidative stress and mitochondrial dysfunction[33].

Because multiple mechanisms are involved in the pathogenesis of neurodegenerations, we have designed compounds that are aimed at simultaneously combating multiple targets in these complex diseases[34]. We have previously reported the development of an initial series of multifunctional antioxidants (MFAO-1s) where 4-(5-hydroxypyrimidin-2-yl)-*N,N*-dimethyl-3,5-dioxopiperazine-1-sulfonamide (JHX-**4**) and 4-(5-hydroxy-4,6-dimethoxypyrimidin-2-yl)-*N,N*-dimethyl-3,5-dioxopiperazine-1-sulfonamide (JHX-**8**) possess a 2-amino-5-hydroxypyrimidine free radical scavenging group (FRS) and a chelating group (CHL) consisting of two carbonyls directly adjacent to an amino group that function independently[35]. This initial series of MFAO-1s demonstrated protective effects against ROS in human lens epithelial cells (hLECs), retinal pigmented epithelial cells (RPEs), and hippocampal astrocytes[35]. In rats, oral administration of these MFAO-1s significantly delayed the progression of cataracts induced by ROS in diabetes and whole head γ-irradiation[36]. Furthermore, in a rat model of dry atrophic AMD, they demonstrated retinal neuroprotection against light-induced injury where ROS is generated and iron is released from degenerating photoreceptors[37]. While tissue analyses confirmed their presence in the lens and neural retina, their accumulation in the brain was minimal[36, 37].

Here, we report the synthesis and *in vitro* biochemical evaluation of a new series of MFAO-2 that accumulate in the brain following oral administration (Figure 2). This has been achieved by modifying the upper ring portion of MFAO-1s, while retaining the 2-diacetylamino-5-hydroxypyrimidine moieties required for independent antioxidant and metal attenuation activity. These MFAO-2s have subsequently been shown to reduce both $A\beta_{40}$ and $A\beta_{42}$ isoform levels in transgenic JAX Alzheimer's mice by oral administration as well as remove zinc from the Aβ:Zn complex so that Aβ plaques can be subsequently degraded by matrix metalloproteinase-2[38].

■ CHEMISTRY

The upper ring system, 1-*N,N'*-dimethylsulfamoyl piperazine, in the first series of MFAO-1s was replaced with either a succinimide ring or glutarimide ring to give the second series of MFAO-2s as outlined in Scheme 1. According to the established procedure[35], the coupling reaction of the 2-aminopyrimidines **19**-**22** with commercially available succinic anhydride **17** or glutaric anhydride **18** gave the 1-(2-pyrimidyl)pyrrolidine-2,5-dione analogs **1**, **3**, **23**, and **25** or the 1-(2-pyrimidyl)piperidine-2,6-dione analogs **5**, **7**, **24**, and **26**. Removal of the benzyloxy protecting groups by hydrogenation gave the MFAO-2s **2**, **4**, **6**, and **8**. The aminopyrimidines **19** and **20** were obtained as previously described[35] while **21** was commercially available. The amino pyrimidine **22** was obtained from commercially available 2-chloro-4, 6-dimethoxypyrimidine **27** by nucleophilic substitution of the 2-chloropyrimidine with benzylamine followed by hydrogenation as outlined in Scheme 2.

Compounds **9** to **16** were synthesized from the 2-chloropyrimidines **31**, **32**, **33**, and **34** by coupling with commercially available pyrrolidine **29** or piperidine **30** followed by hydrogenation as outlined in Scheme 3. The 2-chloropyrimidines **33** and **34** were commercially available while **32** was obtained as previously described[35]. The 2-chloropyrimidine **31** was obtained from commercially available 2-chloro-5-nitropyrimidine **39** by reduction of the nitro group to amine 5-amino-2-chloropyrimidine **40**, acidic hydroxylation, and subsequent protection of the hydroxyl group as outlined in Scheme 4.

■ RESULTS AND DISCUSSION

In vitro analyses were conducted on the multifunctionals containing an upper ring succinimide ring (**2**, **4**) and glutarimide ring (**6**, **8**), their monofunctional FRS analogs (**10, 12**, and **14**, **16,** respectively), their monofunctional CHL analogs (**1**, **3** and **5**, **7**, respectively) as well as their nonfunctional parent analogs (**9**, **11**, and **13**, **15**, respectively).

Metal Binding Studies. The stoichiometry of the chelator-metal ion complexes was obtained using the method of continuous variation (Job plots) as previously described[35]. Several solutions of each compound and metal ion of interest were examined at a constant total concentration (0.1 - 0.5 mM) of the MFAOs **2**, **4**, **6**, and **8** and their monofunctional chelating analogs **1**, **3**, **5**, and **7** and the ion Fe^{2+}, Fe^{3+}, Cu^{+}, Cu^{2+}, Zn^{2+}, Mn^{2+},Ca^{2+}, and Mg^{2+} by altering the mole fraction of one of the components. As summarized in Table 1, compounds **1-8** bound the transition metals Fe^{2+}, Fe^{3+}, Cu^{+},

Cu^{2+}, Zn^{2+}, and Mn^{2+} in 1:2 ratio; however, these compounds failed to bind Ca^{2+} and Mg^{2+}.

***In Vitro* Evaluation of Cytotoxicity and Antioxidant Activity.** The cytotoxicity of compounds **1-16** was evaluated using a MTS Cell Viability assay in SH-SY5Y human neuroblastoma cells (hNBs) and ARPE -19 human retinal pigmented epithelial cells (RPEs). All cells were exposed for 2 h to 1 mM of the MFAOs **2**, **4**, and **6**, **8**, their monofunctional FRS analogs **10, 12**, and **14**, **16,** respectively, and their monofunctional CHL analogs (**1**, **3**, and **5**, **7**, respectively) as well as their nonfunctional parent analogs **9**, **11**, and **13**, **15**, respectively, as well as the previous MFAO-1 JHX-**4**, the metal attenuator clioquinol (PBT-1), and Trolox, a water-solubilized vitamin E derivative. As shown in Figure 3, no apparent cytotoxicity was observed with either compounds **1-16** or Trolox; however, clioquinol demonstrated a significant 30% reduction of the cell viability in human retinal pigmented epithelial cells (RPEs) and a 20% reduction in human neural neuroblastoma cells (hNBs).

To confirm the protective effect of MFAOs against the reactive hydroxyl radicals, both cells were treated with 1 mM of Fenton reagent (1 mM H_2O_2 and 1 mM Fe^{2+}) with or without 1 mM of compound **1-16**, JHX-**4**, clioquinol, or Trolox. As shown in Figure 4, the multifunctional antioxidants **2**, **4**, **6**, and **8** protected the hNB and RPE cells against hydroxyl radical generated ROS similar to that observed for MFAO-1 JHX-**4**. In both cells, this protection was significantly higher than that of the metal attenuator clioquinol. The activity of Trolox was only less in RPE cells. In order of protection, the MFAOs **2**, **4**, **6**, **8**, and JHX-**4** provided significantly more protection than the monofunctional free

radical scavengers **10**, **12**, **14**, and **16** or Trolox. Even less protection was provided by the monofunctional chelators **1**, **3**, **5**, and **7** or clioquinol and no protection was provided by the non-functional parent compounds **9**, **11**, **13**, and **15**. The cellular levels of reduced GSH, which is a sensitive biomarker of oxidative stress, were also measured under the same conditions as the cell viability experiments. As summarized in Figure 5, cells exposed to MFAOs were able to maintain GSH levels similar to JHX-**4** and these levels were significantly higher than in cells exposed to Trolox or clioquinol. The relative activities of compounds with multifunctional versus monofunctional groups showed results similar to those observed with the viability studies.

The ability of MFAOs to protect cells against superoxide radicals was also assessed in both hNBs and RPEs. Mitochondrial superoxide was generated using xanthine oxidase and the levels of superoxide radicals generated were detected by selective MitoSOX^{TM} Red fluorescence. For these studies, all cells were exposed to xanthine oxidase (XO, 25 mU/mL) for 1 h to generate approximately 100 μM superoxide with/without the presence of either the enzyme superoxide dismutase (SOD) or 1, 10, 100, and 1000 μM of MFAOs **2**, **4**, and JHX-**4**, the non-functional parent compounds **9** and **11**, clioquinol, or Trolox. As shown in Figure 6, superoxide levels generated were reduced by MFAOs, clioquinol and Trolox in a similar dose-dependent manner in both cell lines. A similar dose-dependent cell protection against hydroxyl radicals was also observed using LIVE/DEAD® Viability/Cytotoxicity staining (Figure 7). Exposure to hydroxyl radicals generated by 100 μM Fenton reagent for 2 h resulted in only 40% of RPE and hNBs cells remaining viable. Both cells were protected against hydroxyl radicals by the

dose-dependent presence of MFAOs **2**, **4**, and JHX-**4** or clioquinol; however, the non-functional parent compounds **9** and **11** provided no protection.

Bioavailability Study

Both the first generation MFAOs JHX-**4** and JHX-**8** and the second generation MFAOs **2**, **4**, **6**, and **8** were administered to C57BL/6 mice by feeding chow containing 0.05% of the each compound for 14 days. Consumption studies indicated that this corresponded to an average daily dose of 80 mg/kg. After whole body perfusion at the time of sacrifice, the drug levels in the lens, neural retina, and brain were measured by HPLC-MS. All MFAOs examined showed good oral bioavailability to at least one target tissue. This was anticipated because all compounds with the exception of JHX**-8** which possesses 12 hydrogen bond acceptors comply with Lipinski's Rule of 5[39]. As illustrated in Figure 8A, all MFAO-2s accumulated in the brain (60 – 254 ng/mg protein) at 20 to 85-fold higher levels than MFAO-1s (JHX-4, 3 ng/mg protein and JHX-8, 4 ng/mg protein). In contrast, both MFAO-2s and MFAO-1s achieved similar levels in the neural retina (Figure 8B); however, lower levels of MFAO-2s accumulated in the lens than those of MFAO-1 (Figure 8C). While it has generally been assumed that more lipophilic compounds should easily get into both the brain and the avascular lens, the present results suggest that differences exist in the passage of lipophilic drugs through the blood aqueous barrier that is required to reach the lens and the blood brain barrier that is required to reach the brain. Ongoing studies are investigating the molecular physicochemical parameters of these compounds that are associated with their uptake into the retina, brain, and lens.

■ CONCLUSION

Replacing the *N, N*-dimethyl-piperazine-1-sulfonamide group in the first generation of multifunctional antioxidants with either a pyrrolidine or piperidine ring resulted in a new class of multifunctional antioxidants that have increased bioavailability to the brain. These second generation multifunctional antioxidants retain both the FRS activity against ROS and metal attenuation activity and protected hNBs and RPEs against both hydroxyl and superoxide radicals. While both generations of multifunctionals demonstrated similar retinal bioavailability, distinct differences in uptake to lens and brain were observed. The MFAO-2s demonstrated 20-85-fold improved drug penetration to the brain compared to MFAO-1s.These results suggest that MFAO-2 may have coadjutant therapeutic potential for AMD as well as AD since ROS and redox-active metals are all present in these diseases.

■ EXPERIMENTAL SECTION

General. All solvents and reagents were obtained from commercial sources in highest purity available. Clioquinol was purchased from TCI (>98%, Tokyo, Japan) and further purified by recrystallization. NMR spectra were obtained with a Varian 500 MHz spectrometer. Uncorrected melting points were obtained with the Melting Point Apparatus MPA-120 EZ-Melt (Stanford Research Systems, Sunnyvale, CA). Column chromatography (CC) utilized SELECTO SCIENTIFIC silica gel (200-400 mesh). UV-visible spectra were measured on a Molecular Devices SpectraMax Plus384 microplate spectrophotometer (Molecular Devices, Sunnyvale, CA). Final compound purities were assessed as ≥99% and intermediate compound purities were assessed as ≥96% by

reverse phase HPLC using a 250 mm x 4.6 mm C18 Luna 5 μm column (Phenomenex Inc., Torrance, CA) with a mobile phase of 75:25 methanol/water at a flow rate of 0.9 mL/min and detection at 220, 254, and 280 nm. Elemental analyses were done by M-H-W Laboratories, Phoenix, AZ.

***N*-benzyl-4,6-dimethoxypyrimidin-2-amine** (**28**)**.** A mixture of 2-chloro-4,6-dimethoxypyrimidine (**27**) (50.0 g, 0.29 mol), $BnNH_2$ (93.3 mL, 0.85 mol) and K_2CO_3 (62.5 g, 0.45 mol) in dioxane (1.0 L) was refluxed for 4 days. The reaction was filtered and the filtrate concentrated *in vacuo* to give a yellow oil. Silica gel column chromatography with 20:1 to 10:1 hexanes:EtOAc gave 61.7 g (87%) of white solid **28**. ^{1}H NMR ($CDCl_3$) δ 7.36-7.27 (m, 5H), 5.42 (s, 1H), 5.25 (s, 1H), 4.61 (d, *J*=5.86Hz, 2H), 3.83 (s, 6H).

2-amino-4,6-dimethoxypyrimidine (**22**)**.** Compound **28** (27.0 g, 0.11 mol) in 400 mL of MeOH was hydrogenated for 2 days at r.t. in the presence of 5.4 g of 20% $Pd(OH)_2$ catalyst under 1 atmosphere of hydrogen gas (balloon). After filtration, and solvent evaporation, a white solid was obtained which after silica gel column chromatography using 50:1 $CHCl_3$:MeOH yielded 16.8 g (98%) of **22**. ^{1}H NMR ($CDCl_3$) δ 5.47 (s, 1H), 4.90 (s, 2H), 3.84 (s, 6H).

General Procedure for the Preparation of 1-(2-pyrimidyl)pyrrolidine-2,5-dione (1), 1-(4,6-dimethoxy-2-pyrimidyl) pyrrolidine-2,5-dione (3), 1-(2-pyrimidyl)piperidine-2,6-dione (5), 1-(4,6-dimethoxy-2-pyrimidyl)piperidine-2,6-dione (7), 1-(5-benzyloxy-2-pyrimidyl)-pyrrolidine-2,5-dione (23), 1-(5-benzyloxy-2-pyrimidyl)-piperidine-2,6-dione (24), 1-(4,6-dimethoxy-5-benzyloxy-2-pyrimidyl)pyrrolidine-

2,5-dione (25), 1-(4,6-dimethoxy-5-benzyloxy-2-pyrimidyl)-piperidine-2,6-dione (26). 42.0 g (0.42 mol) of succinic anhydride (**17**) dissolved in 300 mL of toluene, 20 g (0.21 mol) of 2-aminopyrimidine (**21**) dissolved in 200 mL of acetone was added and the mixture was heated to 85 ^{o}C for 3 days. After cooling to r.t., the precipitated product was filtered and washed with toluene. The filtrate was dried *in vacuo*, and the dried product was then dissolved in 300 mL of anhydrous Ac_2O and again heated to 85 ^{o}C for 3 h. After removal of the remaining Ac_2O *in vacuo*, the product was purified by silica gel column chromatography with $CHCl_3$ and recrystallized from EtOAc to give compound **1** as a white solid, mp 148.5-149.5 ^{o}C in 32% yield. ^{1}H NMR ($CDCl_3$) δ 8.92 (d, *J*=4.88Hz, 2H), 7.42 (t, *J*=4.88Hz, 1H), 2.96 (s, 4H); Anal. Calcd for $C_8H_7N_3O_2$: C, 54.24; H, 3.98; N, 23.72. Found: C, 54.29; H, 4.19; N, 23.90.

Compound **3** was obtained as a white solid, mp 166.9-168.7 ^{o}C, in 60% yield. ^{1}H NMR ($CDCl_3$) δ 6.09 (s, 1H), 3.94 (s, 6H), 2.92 (s, 4H); Anal. Calcd for $C_{10}H_{11}N_3O_4$: C, 50.63; H, 4.67; N, 17.71. Found: C, 50.78; H, 4.80; N, 17.80.

Compound **5** was obtained as a white solid, mp 220.8-221.3 ^{o}C, in 51% yield. ^{1}H NMR ($CDCl_3$) δ 8.88 (d, *J*=4.88Hz, 2H), 7.40 (t, *J*=4.88Hz, 1H), 2.83 (t, *J*=4.59Hz, 4H), 2.18-2.15 (m, 2H); Anal. Calcd for $C_9H_9N_3O_2$: C, 56.54; H, 4.74; N, 21.98. Found: C, 56.77; H, 4.85; N, 21.70.

Compound **7** was obtained as a white solid, mp 229.2-232.4 ^{o}C, in 63% yield. ^{1}H NMR ($CDCl_3$) δ 6.06 (s, 1H), 3.92 (s, 6H), 2.79 (t, *J*=6.59Hz, 4H), 2.15-2.12 (m, 2H); Anal. Calcd for $C_{11}H_{13}N_3O_4$: C, 52.59; H, 5.22; N, 16.73. Found: C, 52.60; H, 5.40; N, 16.63.

Compound **23**, purified by silica gel column chromatography using 100:1 $CHCl_3$:MeOH as eluent, was obtained as a white solid in 86% yield. ^{1}H NMR ($CDCl_3$) δ 8.57 (s, 2H), 7.44-7.43 (m, 5H), 5.21 (s, 2H), 2.93 (s, 4H).

Compound **24**, purified with silica gel column chromatography using 100:1 $CHCl_3$:MeOH as eluent, was obtained as a white solid in 70% yield. ^{1}H NMR ($CDCl_3$) δ 8.54 (s, 2H), 7.44-7.39 (m, 5H), 5.19 (s, 2H), 2.81 (t, *J*=6.59Hz, 4H), 2.17-2.13(m, 2H).

Compound **25,** purified by silica gel column chromatography with 100:1 $CHCl_3$:MeOH as eluent, was obtained as a white solid in 73% yield. ^{1}H NMR ($CDCl_3$) δ 7.44-7.31 (m, 5H), 5.07 (s, 2H), 3.96(s, 6H), 2.28 (s, 4H).

Compound **26,** purified by silica gel column chromatography with 100:1 $CHCl_3$:MeOH, was obtained as a white solid in 63% yield. ^{1}H NMR ($CDCl_3$) δ 7.47-7.35 (m, 5H), 5.03 (s, 2H), 3.96 (s, 6H), 2.80 (t, *J*=6.59Hz, 4H), 2.15-2.13(m, 2H).

General Procedure for the Preparation of 1-(5-hydroxy-2-pyrimidyl) pyrrolidine-2,5-dione (2), 1-(4,6-dimethoxy-5-hydroxy-2-pyrimidyl)pyrrolidine-2,5-dione (4), 1-(5-hydroxy-2-pyrimidyl)piperidine-2,6-dione (6), 1-(4,6-dimethoxy-5-hydroxy-2-pyrimidyl)-piperidine-2,6-dione (8). Compound **23** (14.7 g, 51.9 mmol) dissolved in 750 mL of acetone was hydrogenated with 3.7 g of 10% Pd/C catalyst at r.t. for 12 h 1 atmosphere of hydrogen gas (balloon). After filtration and solvent evaporation, compound **2** was obtained as a white fluffy solid. Following recrystallization with i-PrOH, 10 g of **2,** mp 278.0-280.0 ^{o}C, was obtained in 76% yield. ^{1}H NMR (DMSO-d_6) δ 11.02

(s, 1H), 8.46 (s, 2H), 2.85 (s, 4H); Anal. Calcd for $C_8H_7N_3O_3$: C, 49.74; H, 3.65; N, 21.75. Found: C, 50.00; H, 3.69; N, 21.54.

Compound **4** was obtained as a white solid, mp 193.7-195.0 ^oC, in 91% yield after recrystallization from Et_2O. ^1H NMR ($CDCl_3$) δ 5.15 (s, 1H), 4.03 (s, 6H), 2.91 (s, 4H); Anal. Calcd for $C_{10}H_{11}N_3O_5$: C, 47.43; H, 4.38; N, 16.59. Found: C, 47.53; H, 4.48; N, 16.58.

Compound **6** was obtained as a white solid, mp 243.5-244.3 ^oC, in 89% yield after recrystallization from acetone. ^1H NMR (DMSO-d_6) δ 10.85 (s, 1H), 8.39 (s, 2H), 2.75 (t, *J*=6.35Hz, 4H), 1.99-1.96 (m, 2H); Anal. Calcd for $C_9H_9N_3O_3$: C, 52.17; H, 4.38; N, 20.28. Found: C, 52.14; H, 4.52; N, 20.04.

Compound **8** was obtained as a white solid, mp 222.0-224.0 ^oC, in 86% yield after recrystallization from Et_2O. ^1H NMR ($CDCl_3$) δ 6.06 (s, 1H), 3.92 (s, 6H), 2.80 (t, *J*=6.59Hz, 4H), 2.15-2.13 (m, 2H); Anal. Calcd for $C_{11}H_{13}N_3O_5$: C, 49.44; H, 4.90; N, 15.72. Found: C, 49.52; H, 4.99; N, 15.65.

General Procedure for the Preparation of 2-(pyrrolidine-1-yl)pyrimidine (9), 4,6-dimethoxy-2-(pyrrolidine-1-yl)pyrimidine (11), 2-(piperidine-1-yl)pyrimidine (13), 4,6-dimethoxy-2-(piperidine-1-yl)pyrimidine (15), 5-benzyloxy-2-(pyrrolidine-1-yl)pyrimidine (35), 5-benzyloxy-2-(piperidine-1-yl)pyrimidine (36), 5-benzyloxy-4,6-dimethoxy-2-(pyrrolidine-1-yl)pyrimidine (37), 5-benzyloxy-4,6-dimethoxy-2-(piperidine-1-yl)pyrimidine (38). To 9.53 mL (116 mmol) pyrrolidine (**29**) in 400 mL of anhydrous THF was added 2.78 g of sodium hydride (116 mmol) and the mixture was

refluxed for 0.5 h. After cooling to r.t., 12 g (105 mmol) of 2-chloropyrimidine (**33**) was added dropwise and the mixture was refluxed for 2 days and then cooled in an ice bath. Water (200 mL) was then added to the cooled reaction mixture and the THF was removed *in vacuo.* The aqueous residue was extracted with $CHCl_3$ and the combined $CHCl_3$ extracts were washed with brine, dried over magnesium sulfate, and filtered. After removal of solvent *in vacuo*, the residue was purified by silica gel column chromatography using 20:1 hexanes: EtOAc as eluent. The product was then recrystallized from Et_2O to give a 12.0 g (76%) of compound **9** as a yellow solid, mp 39.0-39.6 ^oC . ^1H NMR ($CDCl_3$) δ 8.31 (d, *J*=4.88Hz, 2H), 6.45 (t, *J*=4.88Hz, 1H), 3.57 (t, *J*=4.4Hz, 4H), 2.01-1.98 (m, 4H). Anal. Calcd for $C_8H_{11}N_3$: C, 64.40; H, 7.43; N, 28.16. Found: C, 64.42; H, 7.53; N, 27.97.

Compound **11** was obtained as a white solid, mp 63.3-63.7 ^oC, 71% yield after recrystallization from Et_2O. ^1H NMR ($CDCl_3$) δ 5.34 (s, 1H), 3.87 (s, 6H), 3.56 (t, *J*=6.59Hz, 4H), 1.93-1.96 (m, 4H); Anal. Calcd for $C_{10}H_{15}N_3O_2$: C, 57.40; H, 7.23; N, 20.08. Found: C, 57.20; H, 7.03; N, 19.91.

Compound **13** was obtained as a colorless oil in 90% yield after vacuum distillation at 90˚C under 0.25 mmHg. ^1H NMR ($CDCl_3$) δ 8.22 (d, *J*=4.64Hz, 2H), 6.35 (t, *J*=4.64Hz, 1H), 3.71 (t, *J*=5.37Hz, 4H), 1.64-1.58 (m, 2H), 1.56-1.51 (m, 4H); Anal. Calcd for $C_9H_{13}N_3$: C, 66.23; H, 8.03; N, 25.74. Found: C, 66.49; H, 7.95; N, 25.81.

Compound **15** was obtained as a white solid mp 59.8-60.4˚C in 74% yield. ^1H NMR ($CDCl_3$) δ 5.25 (s, 1H), 3.77 (s, 6H), 3.68 (t, *J*=5.49Hz, 4H), 1.60-1.55 (m, 2H), 1.52-

1.48 (m, 4H); Anal. Calcd for $C_{11}H_{17}N_3O_2$: C, 59.17; H, 7.67; N, 18.82. Found: C, 58.94; H, 7.49; N, 18.56.

Compound **35** was obtained in 86% yield. ^{1}H NMR ($CDCl_3$) δ 8.06 (s, 2H), 7.34-7.25 (m, 5H), 4.93 (s, 2H), 3.45 (t, *J*=6.59Hz, 4H), 1.93-1.90 (m, 4H).

Compound **36** was obtained in 75% yield. ^{1}H NMR ($CDCl_3$) δ 8.04 (s, 2H), 7.33-7.25 (m, 5H), 4.94 (s, 2H), 3.63 (t, *J*=4.88Hz, 4H), 1.58-1.52 (m, 6H).

Compound **37** was obtained in 80% yield. ^{1}H NMR ($CDCl_3$) δ 7.47-7.32 (m, 5H), 4.84 (s, 2H), 3.90 (s, 6H), 3.51 (t, *J*=6.59Hz, 4H), 1.95-1.92 (m, 4H).

Compound **38** was obtained in 75% yield. ^{1}H NMR ($CDCl_3$) δ 7.46-7.27 (m, 5H), 4.85 (s, 2H), 3.89 (s, 6H), 3.69 (t, *J*=5.49Hz, 4H), 1.66-1.57 (m, 6H).

General procedure of preparation of 5-hydroxy-2-(pyrrolidine-1-yl)pyrimidine (10), 5-hydroxy-4,6-dimethoxy-2-(pyrrolidine-1-yl)pyrimidine (12), 5-hydroxy-2-(piperidine-1-yl)pyrimidine (14), 5-hydroxy-4,6-dimethoxy-2-(piperidine-1-yl)pyrimidine (16). Hydrogenation at r.t. for 12 h of compound **38** (17.6 g, 53.4 mmol) dissolved in 350 mL of acetone with 4.4 g of 10% Pd/C catalyst under a one atmosphere of hydrogen gas (balloon) gave compound **16** as a pale red solid after filtration and solvent evaporation. Recrystallization from Et_2O gave 12.7 g (80%) of **16**, mp 120.1-120.5 ^{o}C. ^{1}H NMR (DMSO-d_6) δ 7.63 (brs, 1H), 3.81 (s, 6H), 3.59 (t, *J*=5.25Hz, 4H), 1.60-1.56 (m, 2H), 1.52-1.47 (m, 4H); Anal. Calcd for $C_{11}H_{17}N_3O_3$: C, 55.22; H, 7.16; N, 17.56. Found: C, 55.15; H, 7.21; N, 17.48.

Compound **10** was obtained as a pale yellow solid, mp 151.5-151.8 ^{o}C in 84% yield after recrystallization from Et_2O. ^{1}H NMR ($CDCl_3$) δ 8.05 (s, 2H), 3.55-3.75 (m, 4H), 1.96-1.92 (m, 4H). Anal. Calcd for $C_8H_{11}N_3O$: C, 58.17; H, 6.71; N, 25.44. Found: C, 57.92; H, 6.67; N, 25.18.

Compound **12** was obtained as a yellow solid, mp 108.7-109.2˚C, in 78% yield after recrystallization from Et_2O. ^{1}H NMR (DMSO-d_6) δ 7.49 (brs, 1H), 3.82 (s, 6H), 3.41 (t, *J*=6.47Hz, 4H), 1.89-1.86 (m, 4H); Anal. Calcd for $C_{10}H_{15}N_3O_3$: C, 53.32; H, 6.71; N, 18.66. Found: C, 53.51; H, 6.80; N, 18.80.

Compound **14** was obtained as a pale red solid, mp 94.3-94.7 ^{o}C, in 79% yield after recrystallization from Et_2O. ^{1}H NMR ($CDCl_3$) δ 8.06 (s, 2H), 3.47 (t, J=6.59Hz, 4H), 1.70-1.40 (m, 6H). Anal. Calcd for $C_9H_{13}N_3O$: C, 60.32; H, 7.31; N, 23.45. Found: C, 60.15; H, 7.25; N, 23.26.

5-amino-2-chloropyrimidine (40). 140 g (0.88 mol) of 2-chloro-5-nitropyrimidine (**39**) dissolved in 700 mL of EtOH, 197 g of iron powder (70m mesh, < 212 μm), 700 mL of water, and 1400 mL of acetic acid were added together. The mixture was heated at 70˚C overnight, then cooled to r.t., and then filtered. EtOH was removed from the filtrate *in vacuo*, and the pH was adjusted to 8 with 12 N NaOH and the product was extracted overnight with continuous liquid-liquid extraction with EtOAc. The resulting filter cake was washed with EtOAc, and the combined EtOAc layers were washed with water, then brine, dried over magnesium sulfate, and filtered. After removal of the solvent *in vacuo* and recrystallization with EtOH, 97.2 g (85%) of pale brown solid product **40** was obtained. ^{1}H NMR (DMSO-d_6) δ 8.94 (s, 2H), 5.77 (brs, 2H).

2-chloropyrimidine-5-ol (41). Compound **40** (40 g, 0.31 mol) in 2N sulfuric acid was refluxed for 2 h. After cooling to r.t., the reaction mixture was extracted with EtOAc using continuous overnight liquid-liquid extraction. The combined EtOAc layers were washed with brine, dried over magnesium sulfate, and filtered. After solvent removal *in vacuo* and recrystallization with EtOH, 10 g (25%) yellow solid **41** was obtained. ^{1}H NMR (DMSO-d_6) δ 10.93 (brs, 1H), 6.45 (t, *J*=4.88Hz, 1H), 3.57 (t, *J*=4.4Hz, 4H), 2.01-1.98 (m, 4H).

2-chloro-5-benzyloxy-pyrimidine (31). Potassium carbonate (11.6 g, 84.3 mmol) was added to 10 g of the alcohol **41** (76.6 mmol) in 500 mL of MeOH, followed by benzyl bromide (10.1 mL, 84.3 mmol). After 14 h stirring at r.t., the reaction was stopped by addition of water (300 mL). MeOH was evaporated and the remaining aqueous layer was extracted with $CHCl_3$. The combined $CHCl_3$ layers were washed with brine, dried over magnesium sulfate, and filtered. Removal of the solvent followed by silica gel chromatography using 100:1 $CHCl_3$:MeOH as eluent gave 15 g (89%) of 2-amino-5-benzyloxy-pyrimidine (**31**) as a white solid. ^{1}H NMR ($CDCl_3$) δ 8.27 (s, 2H), 7.37-7.30 (m, 5H), 5.09 (s, 2H).

Metal Binding Studies. The stoichiometry of complexes formed between compounds **1-8** and the ions Cu^+, Cu^{2+}, Fe^{2+}, Fe^{3+}, Zn^{2+}, Mn^{2+}, Ca^{2+}, and Mg^{2+} at a constant total concentration (0.1 - 0.5 mM) were determined as previously described[35] using the method of continuous variation (Job plots) [40]. Due to their low solubility, compounds **1**-**8** were first dissolved in acetonitrile (HPLC grade, UV cutoff 200 nm). These concentrated solutions were then diluted to 0.1 mM stock solutions with 1 mM acetate, pH 6.5). In a

typical experiment (at 23°C), several solutions of the compound and metal ion of interest were prepared at a constant total concentration of compound and ion, but with a different mole fraction of one component. After an equilibration period of 45 minutes, the change in UV absorbance was monitored from 210 to 310 nm (Perkin Elmer Lambda 10 spectrophotometer). The maximum absorbance for each compound was then recorded as a function of the mole fraction of the metal ion. Two linear dependences were obtained, at low and high molar fractions, which intersect at a mole fraction value that corresponds to the stoichiometry of the complex.

Cell Culture Studies. SH-SY5Y human neuroblastoma cells (hNBs, American Type Culture Collection (ATCC, Manassas, VA) and ARPE-19 human retinal pigmented epithelial cells (RPEs, ATCC) were cultured at 37^{o}C under a 5% CO_2 atmosphere in cell media (1:1 Eagles minimum essential medium with Earle's balanced salt solution and Ham's F12 (EMEM-F12) media containing 10% fetal bovine serum (FBS) for hNBs and Dulbecco's modified Eagle's medium (DMEM) containing 4% FBS for RPEs. Both media contained 1% penicillin/streptavidin solution. The cells were passaged when 80-90% confluent by treatment with trypsin-EDTA and then plated at a density of 1x10^4 cells on to 96-well plates or 1x10^6 cells on to 150 mm dishes.

In vitro cell viability studies were conducted as previously described[35] using the Cell Titer 96® Aqueous One Solution Cell Proliferation Assay (MTS, Promega, Madison, WI) with 2 h of exposure to 1 mM of Fenton reagent (1 mM H_2O_2 and 1 mM Fe^{2+}) with/without 1 mM of either compounds **1-16**, JHX-**4**, Trolox, or clioquinol dissolved in 0.16% DMSO. The results were normalized to blank control (100%) of cells not treated with Fenton reagent. On cells cultured in either 60 or 150 mm dishes also, glutathione

(GSH) measurements were conducted as previously described[35] with same exposure as above.

Superoxide Assays were conducted in 96-well plates using the MitoSOX™ Red reagent (Life Technologies Corporation, Carlsbad, CA). After removing cell media and washing with phosphate buffered saline (PBS), cells were preincubated in fresh media (150 μL) without FBS containing 1, 10, 100, or 1000 μM of each compound **2**, **4**, **9**, **11**, JHX-**4**, clioquinol, Trolox, or 25 μg/mL of superoxide dismutase (approximately 100 μM) at 37 °C for 1 h. Xanthine oxidase (100 mU/mL, 50 μL) which generates approximately 100 μM of superoxide was added and cultured for an additional hour. After removing the media and washing with PBS, the cells were stained with 100 μL of the MitoSOX Red reagent (5 μM) and incubated for 2 h. The fluorescence of the each well was measured using fluorescent microplate reader at Ex/Em = 510/580 nm.

LIVE/DEAD® viability/cytotoxicity assays were conducted in 96-well plates using the LIVE/DEAD® Viability/Cytotoxicity Assay kit (Life Technologies Corporation). After removing cell media and washing with PBS, cells were preincubated in fresh media (210 μL) without FBS containing 1, 10, 100, or 1000 μM of each compound **2**, **4**, **9**, **11**, JHX-**4**, clioquinol, or Trolox, at 37 °C for 1h. Fenton reagent (Fe^{2+} and hydrogen peroxide dissolved in appropriate media without FBS to give a final concentration of 100 μM, 40 μL) was added to each well and incubation continued. After 2 h of incubation with Fenton reagent, the media was removed and the cells were washed with PBS. The cells were stained with 100 μL of the LIVE/DEAD reagent containing calcein AM (AM, 8 μM) and ethidium homodimer-1 (EthD-1, 16 μM) for 15 min at 37 °C. The fluorescence

of each well was measured with a fluorescent microplate reader at Ex/Em = 494/517 nm (Fsam for LIVE Cells) and Ex/Em = 528/617 nm (Fsam for DEAD Cells). The fluorescence of control samples were also measured as follows: Fmax for LIVE Cells (The fluorescence at Ex/Em = 494/517 nm in live cells samples labeled with AM only); Fmin for LIVE Cells (The fluorescence at Ex/Em = 494/517 nm in live cells samples labeled with EthD-1 only); Fmax for DEAD Cells (The fluorescence at Ex/Em = 528/617 nm in dead cells samples labeled with EthD-1 only); Fmin for DEAD Cells (The fluorescence at Ex/Em = 528/617 nm in dead cells samples labeled with AM only); Blank494/517 (The fluorescence at Ex/Em = 494/517 nm without dye and cells); Blank528/617 (The fluorescence at Ex/Em = 528/617 nm without dye and cells). For the dead cells control, the cells were incubated in 70% of ethanol for 30 min at 37 °C. The percentage of live cells was calculated from the fluorescence readings using the equation

$$\%\ \text{LIVE Cells} = \frac{(F_{\text{sam for LIVE Cells}} - \text{Blank}_{494/517}) - (F_{\text{min for LIVE Cells}} - \text{Blank}_{494/517})}{(F_{\text{max for LIVE Cells}} - \text{Blank}_{494/517}) - (F_{\text{min for LIVE Cells}} - \text{Blank}_{494/517})} \times 100\%$$

The percentage of dead cells was calculated from the fluorescence readings using the equation:

$$\%\ \text{DEAD Cells} = \frac{(F_{\text{sam for DEAD Cells}} - \text{Blank}_{528/617}) - (F_{\text{min for DEAD Cells}} - \text{Blank}_{528/617})}{(F_{\text{max for DEAD Cells}} - \text{Blank}_{528/617}) - (F_{\text{min for DEAD Cells}} - \text{Blank}_{528/617})} \times 100\%$$

Animal Studies. All procedures were performed in strict accordance with the recommendations in the Guide for the Care and Use of Laboratory Animals of the

National Institutes of Health and approved by the Institutional Animal Care and Use Committee of UNMC (Permit Number 11-086-11-FC).

Bioavailability Studies. Bioavailability studies were conducted in C57BL/6 mice (equal sexes, body weight 14-17 g, n = 6) fed chow containing 0.05% of compounds **2**, **4**, **6**, **8**, JHX-**4**, and JHX-**8** for 14 days. Food consumption and body weights were monitored and indicated that each mouse received an average dose of 80 mg/kg/day of drug. Following whole body perfusion with PBS (5 mL) at the time of sacrifice, the lens, neural retina and brain were removed and homogenized in ice-cold 10 mM acetate buffer pH4 (1 mL for 3 lenses and 3 retinas, 3 mL for 2 brains) containing *N,N'*-dimethyl-4-(pyrimidin-2-yl)piperazine-1-sulfonamide (0.5 mM) as the internal standard. The protein concentration in an aliquot of the supernatant was determined according to Bradford[41]. The remaining supernatant was then deproteinized with equal volumes of 20% trichloroacetic acid (TCA). Following an additional centrifugation at 15,000 g for 30 min. at 4°C, the supernatant was transferred to a clean test tube and dried *in vacuo* overnight. The residue was dissolved in chloroform, centrifuged at 15,000 g for 30 min. at 4°C, and dried *in vacuo*. The remaining organic residue containing the internal standard and extracted compounds **2**, **4**, **6**, **8**, JHX-**4**, and JHX-**8** were dissolved in 200 µL of HPLC grade acetonitrile and separated by reverse phase HPLC (Luna 5 µm, C18, 250 mm x 4 mm) column (Phenomenex Inc., Torrance, CA). The samples were eluted with 75% aqueous methanol. The eluent was monitored by UV at 261/273 nm and ESI-MS in negative mode on a Thermo Finnigan LCQ (Thermo Fisher Scientific, Waltham, MA). Samples were quantified against standard curves of compounds **2**, **4**, **6**, **8**, JHX-**4**, and JHX-**8**. All analyses were conducted in triplicate.

Statistical Analysis. Statistical comparisons between groups were performed with ANOVA test (Origin 8.1, OriginLab Corporation, Northampton, MA). Differences with $p < 0.05$ were considered significant.

FIGURES

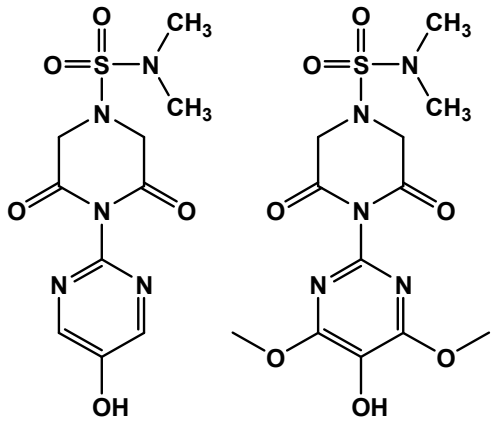

Figure 1. Structures of the first generation of multifunctional antioxidants (MFAO-1)

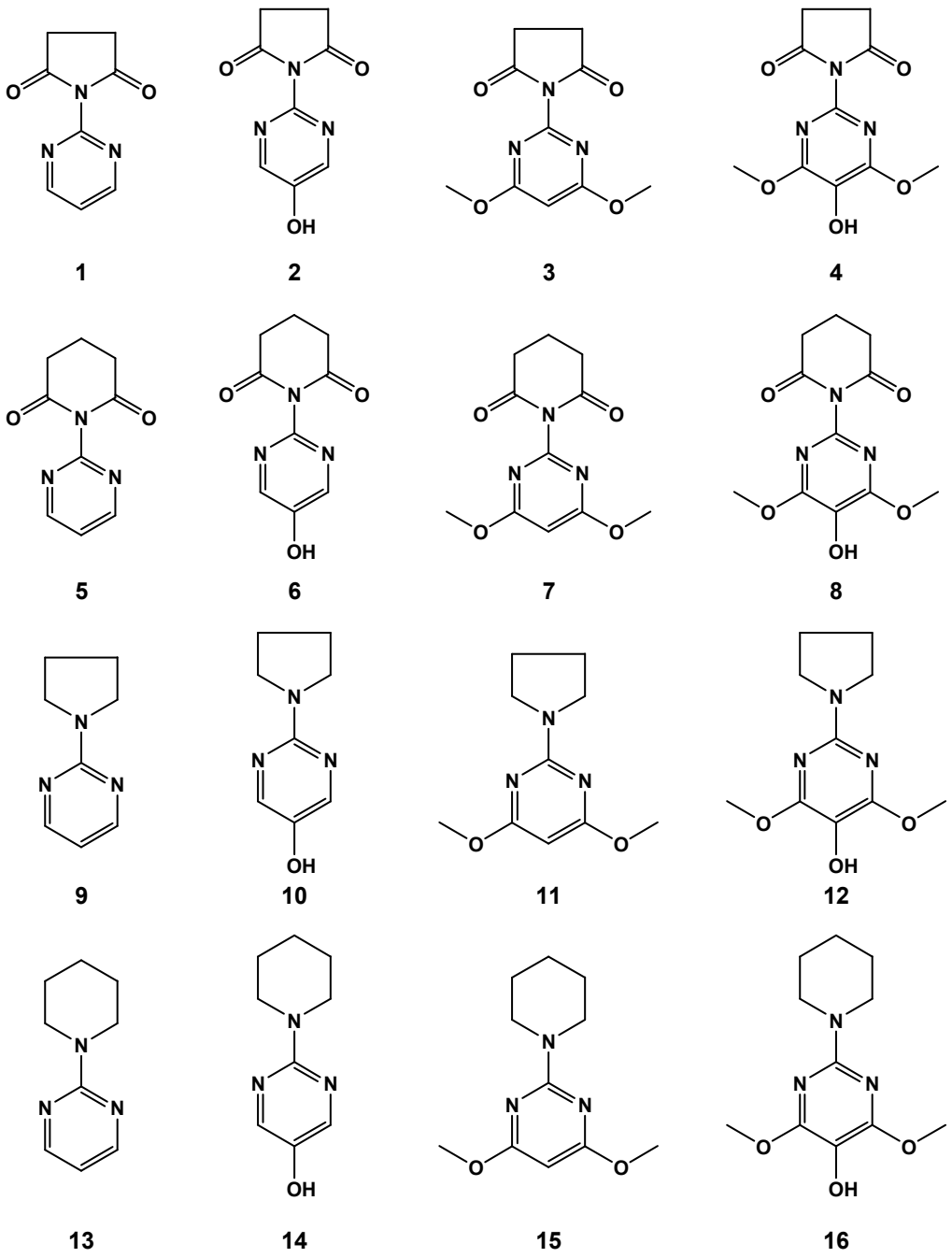

Figure 2. Structures of synthesized compounds in the MFAO-2 series. Shown are multifunctional compounds **2**, **4**, **6**, and **8;** mono-functional chelators (CHL), **1**, **3**, **5**, and **7**; monofunctional free radical scavengers (FRS), **10**, **12**, **14**, and **16**, and the non-functional parent compounds, **9**, **11**, **13**, and **15.**

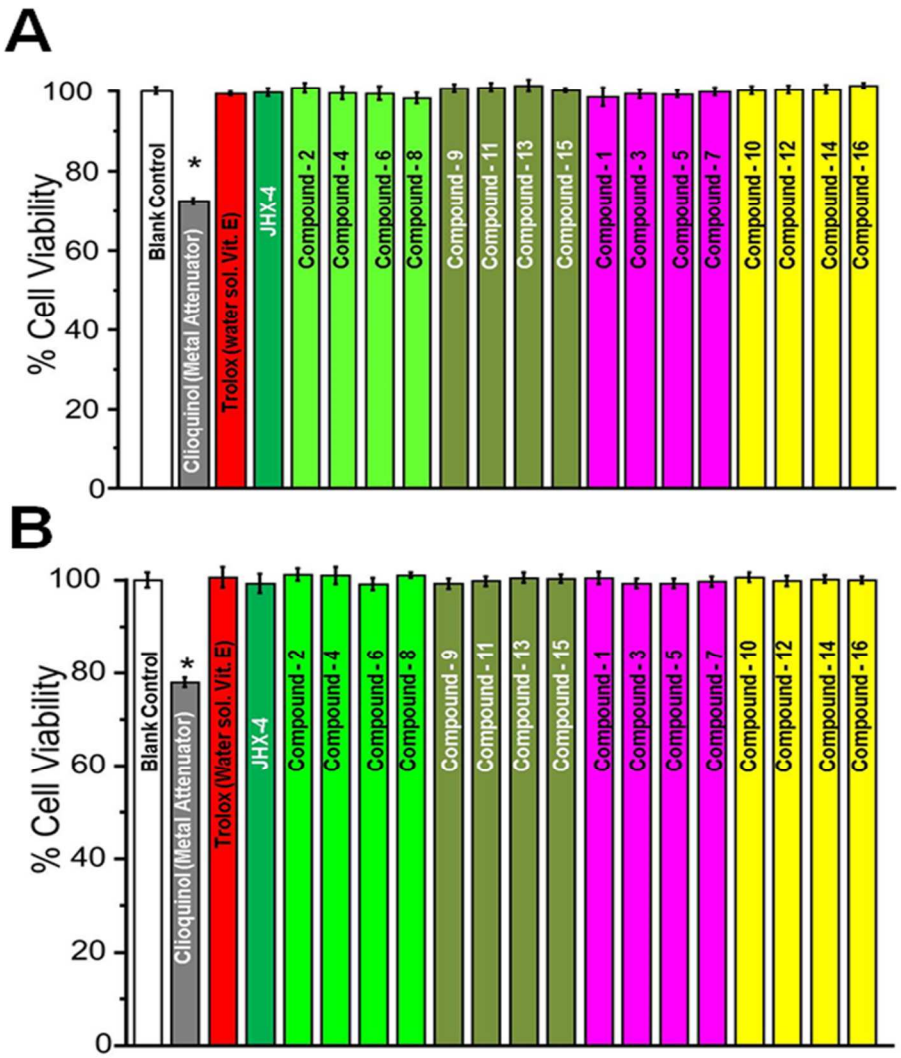

Figure 3. Effect of compound exposure on cell viability of hNBs and RPE cells measured by the MTS viability assay. **A** illustrates the cell viability of RPEs after 2 h exposure to 1 mM of compounds **1-16**, clioquinol, or Trolox. **B** illustrates the cell viability of hNBs after similar exposure to compounds. The results represent the mean ± SEM, n = 4. Significant differences ($p < 0.05$), calculated by ANOVA, were compared to blank control.

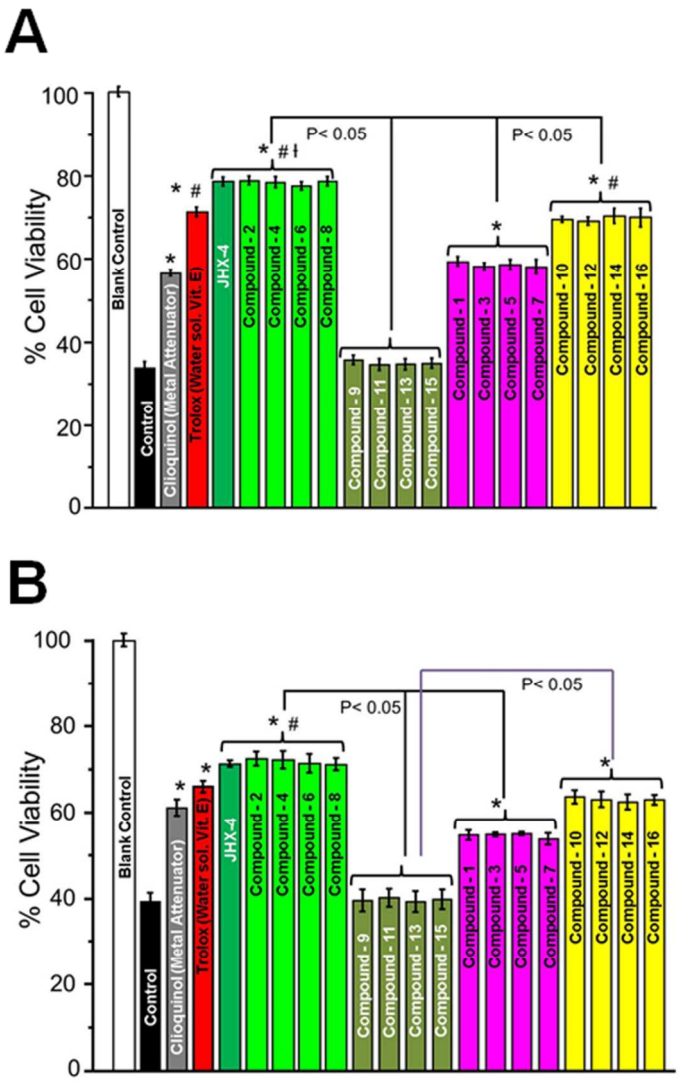

Figure 4. MTS cell viability assay of hNBs and RPEs exposed with/without the presence of compounds to hydroxyl radicals generated via the Fenton reaction. **A** illustrates the cell viability of RPEs exposed for 2 h to 1 mM of Fenton reagent with/without the presence of 1 mM of compounds **1-16**, clioquinol, or Trolox. **B** illustrates the cell viability of similarly exposed hNBs. The results represent the mean ± SEM, n=4. Statistical significant differences, calculated by ANOVA, were as follows: * $p < 0.05$ versus control, # $p < 0.05$ versus clioquinol, and ł $p < 0.05$ versus Trolox.

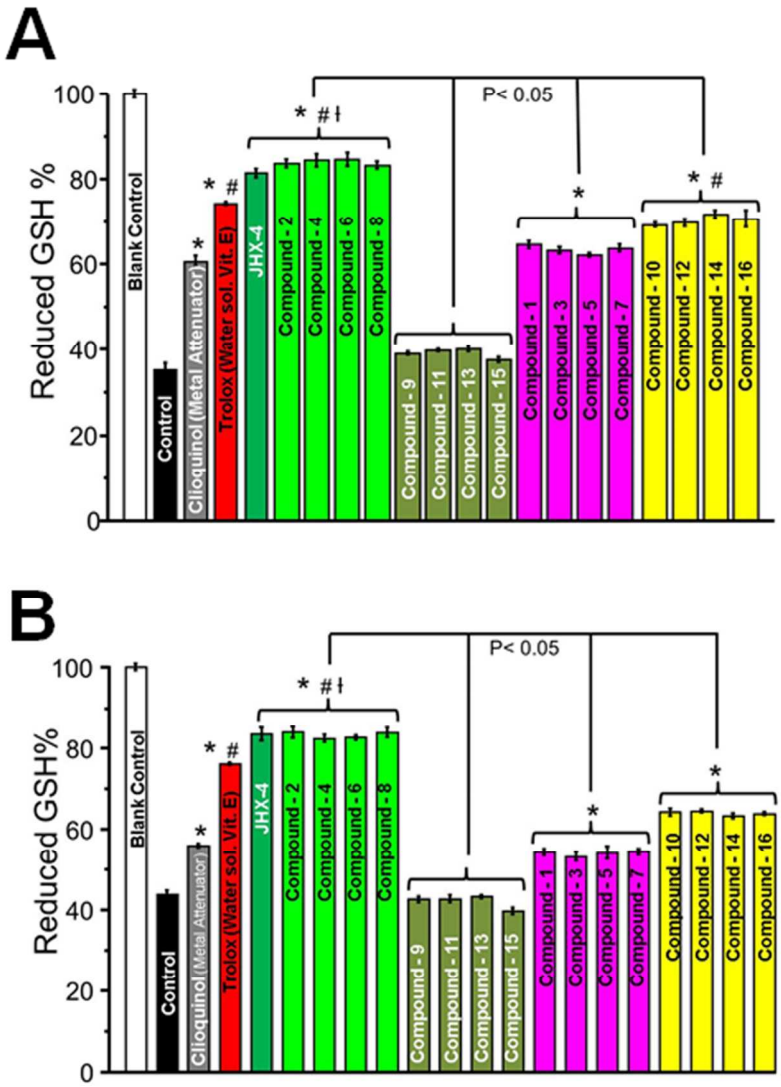

Figure 5. Changes in GSH levels in cells exposed to hydroxyl radicals with/without the presence of compounds **1**-**16**, Trolox, or clioquinol. **B** illustrates GSH levels of RPEs exposed for 2 h with 1 mM of Fenton reagent with/without the presence of 1 mM of compounds **1-16**, clioquinol, or Trolox. **B** illustrates GSH levels of similarly exposed hNB cells. The results represent the mean ± SEM (n = 6). Significant differences, calculated by ANOVA, were as follows: * $p < 0.05$ versus control, # $p < 0.05$ versus clioquinol, and ł $p < 0.05$ versus Trolox.

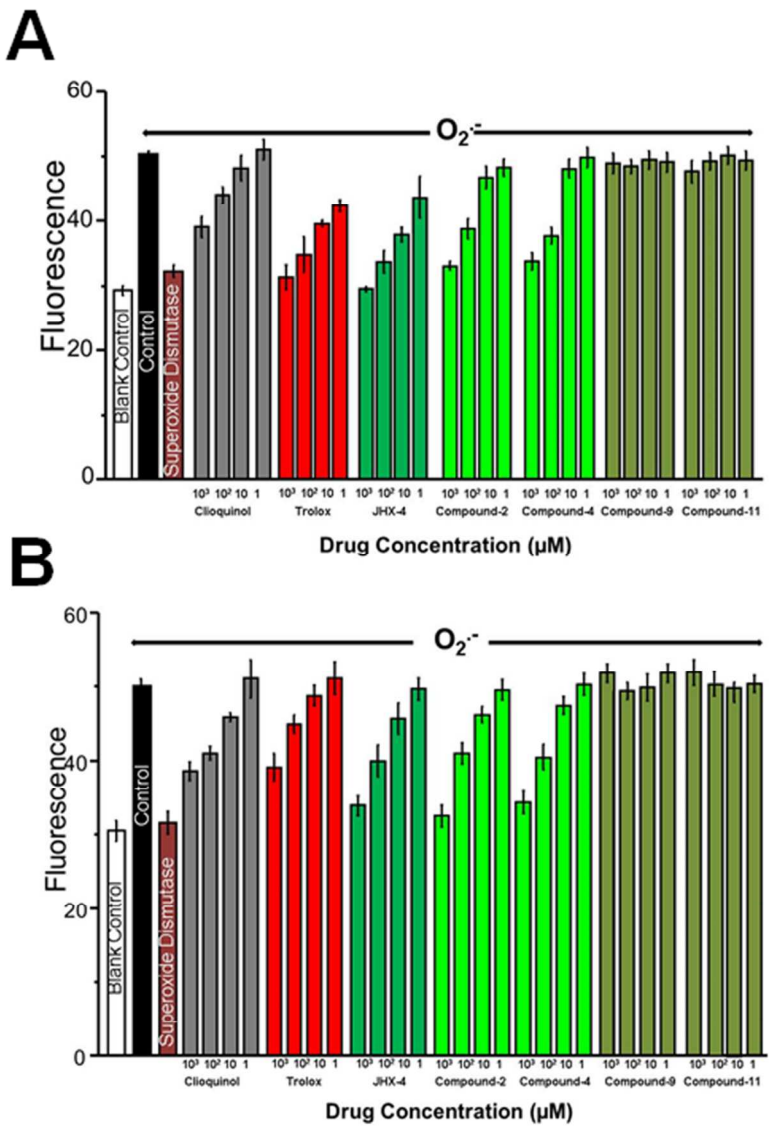

Figure 6. Dose-dependent reduction of superoxide generated by xanthine oxidase and measured by MitoSOX staining in hNB and RPE cells. In **A** hNBs were pre-incubated with/without the presence of 1, 10, 100, 1000 μM compounds **2**, **4**, **9**, **11**, JHX-**4**, clioquinol or Trolox as well as SOD (25 μg/mL, approximately 100 μM) for 1 h and then exposed to xanthine oxidase (25 mU/mL) which can generate approximately 100 μM of superoxide for 1 h. **B** illustrates the results of similar experimental procedures of RPEs. The results represents mean ± SEM, n = 6.

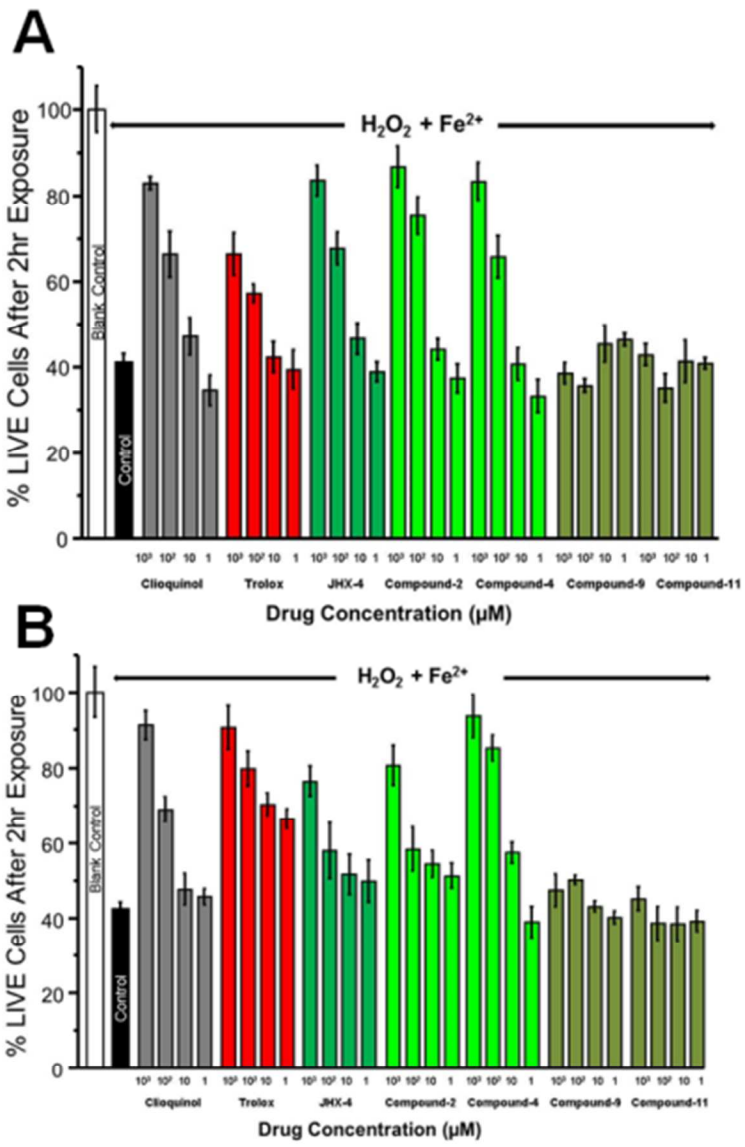

Figure 7. Dose-dependent protection of cells against hydroxyl radicals measured with the LIVE/DEAD Viability Assay. **A** illustrates the results of hNB cells that were pre-incubated for 1 h with/without the presence of 1, 10, 100, 1000 μM of compounds **2**, **4**, **9**, **11**, JHX-**4**, clioquinol, or Trolox for 1 h and exposed to 100 μM Fenton reagent for 2 h. **B** illustrates the results of similar exposure of RPEs as above. The results represents mean ± SEM, n = 6.

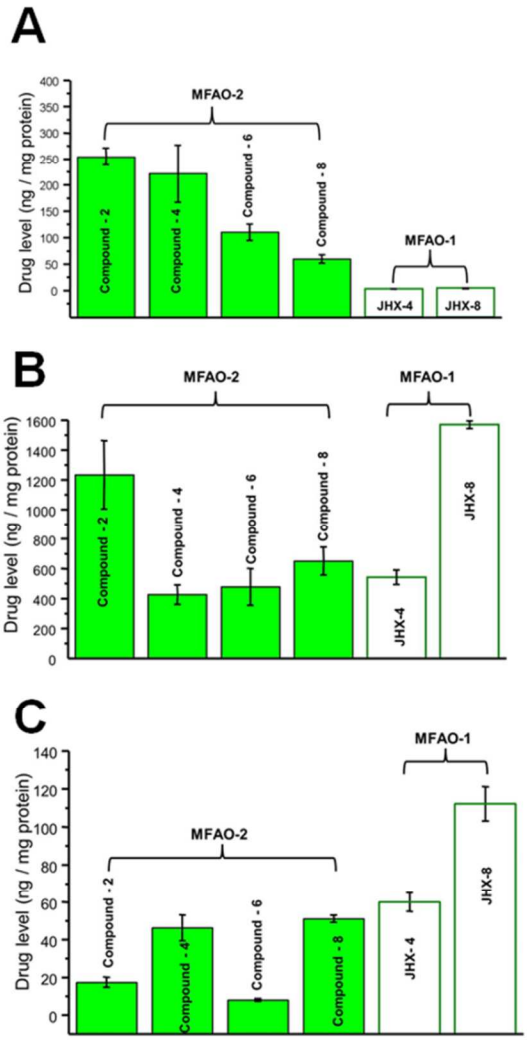

Figure 8. Oral bioavailability of MFAOs in mice. Tissue levels of MFAOs measured in the brain (**A**), neural retina (**B**), and lens (**C**) of C57BL/6 mice fed chow containing 0.05% of each MFAO (80 mg/kg/day average dose) for 14 days. The results represent the mean ± SEM (n = 6-7). The present MFAO-2s achieved higher brain levels compared to the previously synthesized MFAO-1s (**A**) but failed to reach adequate levels in the lens (**C**). Similar neural retinal levels were observed with both MFAO-1 and MFAO-2 (**B**).

SCHEMES

Scheme 1.

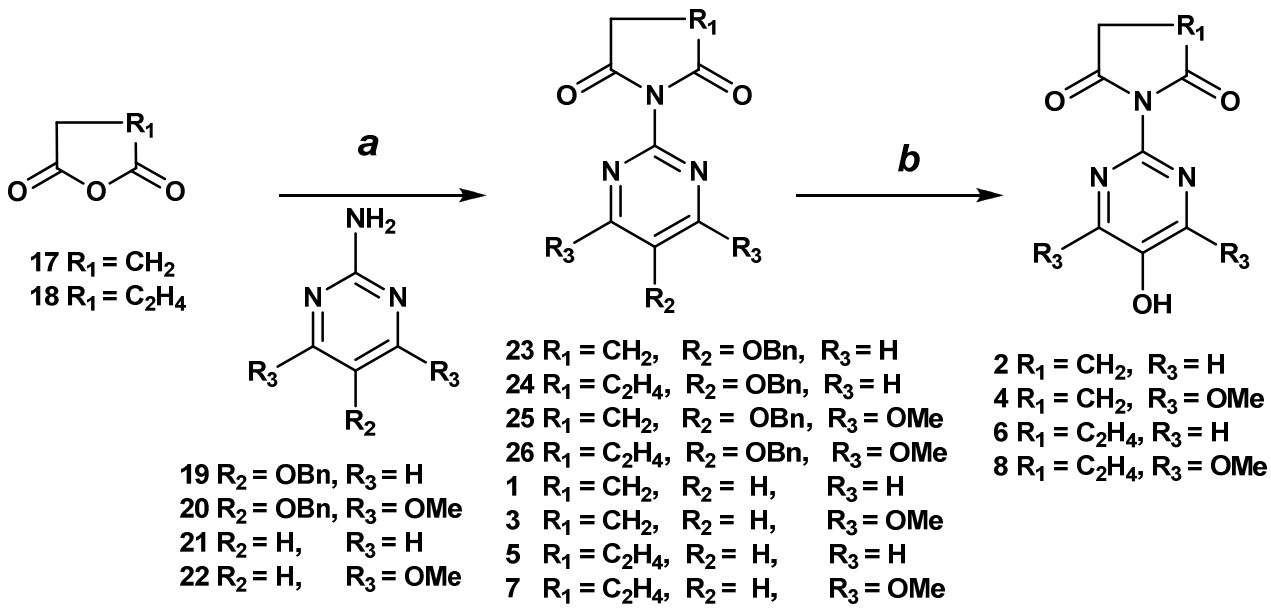

Reagents and conditions: a: 1) acetone/toluene, 85°C; 2) Ac_2O, 85°C; b: Pd-C/H_2/acetone, r.t.

Scheme 2.

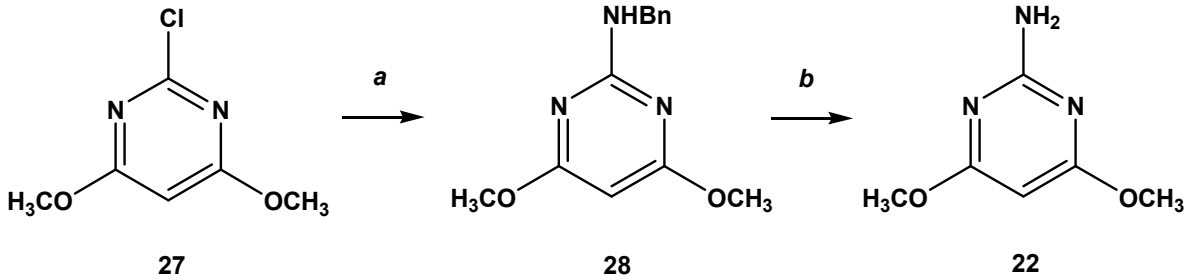

Reagents and conditions: a: $BnNH_2$ / K_2CO_3/ dioxane, reflux; b: 20% $Pd(OH)_2/H_2$/ MeOH, r.t.

Scheme 3.

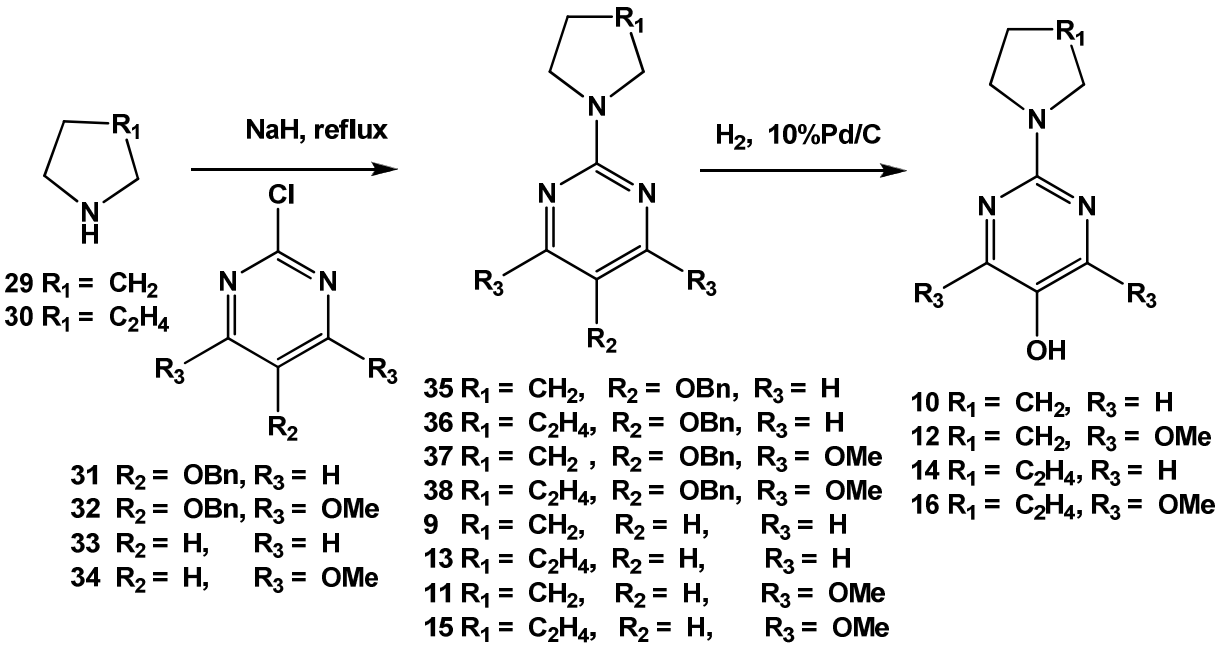

Scheme 4.

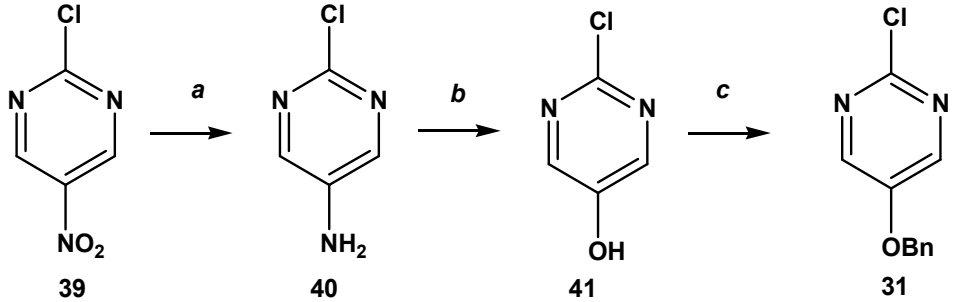

Reagents and conditions: a: Fe/AcOH/EtOH/ H_2O, at 70°C; b: 2M H_2SO_4, reflux; c: BnBr, K_2CO_3/ MeOH, r.t.

TABLES.

Compound	Fe^{2+}	Fe^{3+}	Cu^{+}	Cu^{2+}	Zn^{2+}	Mn^{2+}	Mg^{2+}	Ca^{2+}
1	1.00 : 2.06 ± 0.04	1.00 : 2.01 ± 0.02	1.00 : 2.01 ± 0.17	1.00 : 2.28 ± 0.15	1.00 : 1.87 ± 0.14	1.00 : 1.98 ± 0.07	0*	0*
2	1.00 : 2.06 ± 0.10	1.00 : 2.01 ± 0.05	1.00 : 2.01 ± 0.16	1.00 : 2.28 ± 0.21	1.00 : 1.87 ± 0.14	1.00 : 2.14 ± 0.11	0*	0*
3	1.00 : 2.02 ± 0.08	1.00 : 2.05 ± 0.03	1.00 : 1.92 ± 0.05	1.00 : 2.01 ± 0.16	1.00 : 2.07 ± 0.04	1.00 : 2.04 ± 0.01	0*	0*
4	1.00 : 2.03 ± 0.03	1.00 : 2.12 ± 0.27	1.00 : 2.03 ± 0.14	1.00 : 2.13 ± 0.21	1.00 : 2.01 ± 0.16	1.00 : 2.22 ± 0.05	0*	0*
5	1.00 : 2.13 ± 0.15	1.00 : 1.80 ± 0.03	1.00 : 1.90 ± 0.06	1.00 : 2.01 ± 0.01	1.00 : 2.17 ± 0.08	1.00 : 1.83 ± 0.11	0*	0*
6	1.00 : 1.85 ± 0.07	1.00 : 1.92 ± 0.06	1.00 : 1.86 ± 0.14	1.00 : 1.75 ± 0.05	1.00 : 1.99 ± 0.02	1.00 : 1.91 ± 0.02	0*	0*
7	1.00 : 1.96 ± 0.09	1.00 : 2.08 ± 0.07	1.00 : 1.90 ± 0.03	1.00 : 1.96 ± 0.05	1.00 : 2.06 ± 0.22	1.00 : 1.95 ± 0.24	0*	0*
8	1.00 : 1.97 ± 0.13	1.00 : 1.82 ± 0.05	1.00 : 1.97 ± 0.03	1.00 : 1.86 ± 0.11	1.00 : 2.09 ± 0.13	1.00 : 2.12 ± 0.02	0*	0*

Table 1. Compound to metal ion ratio of select metal ions. The stoichiometry of the compound to metal complexes was obtained from the intersection of lines in Job's plots. The total concentration of the compound **1-8** and metal ion was 0.1 - 0.5 mM. * Non-intersecting lines on the Job Plot. Mean ± S.D.; n=3

ANCILLARY INFORMATION

Table of molecular strings

CORRESPONDING AUTHOR

Peter F. Kador, Ph.D., FARVO

College of Pharmacy, 986025 Nebraska Medical Center

Omaha, NE 68198-6025

Phone: +1-402-559-9261

Email: pkador@unmc.edu

Author Contributions

The manuscript was written by HK as part of his Ph.D. requirement and revised by PK.

All authors have given approval to the final version of the manuscript.

FUNDING SOURCES

Therapeutic Vision, Inc. and Alzheimer's Drug Discovery Foundation

ACKNOWLEDGMENT

The authors than Dr, James Randazzo for his technical advice and Karen Blessing for animal technical assistance.

ABBREVIATIONS

Aβ, amyloid beta; Ac_2O, acetic anhydride; AD, Alzheimer's disease; AMD, age-related macular degeneration; CC, column chromatography; CHL, chelating group; CSF, cerebrospinal fluid; DMSO, dimethyl sulfoxide; EtOAc, ethyl acetate; EtOH, ethanol; Et_2O, ether; FBS, fetal bovine serum; FRS, free radical scavenging group; GSH, reduced glutathione; hLECs, human lens epithelial cells; hNBs, human neuroblastoma cells; HPLC-MS, high performance liquid chromatography-Mass spectrometry; HD, Huntington disease; i-PrOH, *iso*-propanol; JHX-**4**, 4-(5-hydroxypyrimidin-2-yl)-*N,N*-dimethyl-3,5-dioxopiperazine-1-sulfonamide; JHX-**8**, 4-(5-hydroxy-4,6-dimethoxypyrimidin-2-yl)-*N,N*-dimethyl-3,5-dioxopiperazine-1-sulfonamide; MeOH, methanol; MFAOs, multifunctional antioxidants; MFAO-1, first series of multifunctional antioxidants; MFAO-2, second series of multifunctional antioxidants; NMDA, *N*-methyl-D-aspartate; 8-OHQ, 8-hydroxyquinoline; PBS, phosphate buffered saline; RNS, reactive nitrogen species; ROS, reactive oxygen species; RPEs, retinal pigmented epithelial cells; SOD, superoxide dismutase; THF, tetrahydrofuran; XO, xanthine oxidase.

REFERENCES

1. Sies, H. Oxidative stress: oxidants and antioxidants. *Exp Physiol* **1997,** 82, 291-295.
2. Pappolla, M. A.; Omar, R. A.; Kim, K. S.; Robakis, N. K. Immunohistochemical evidence of oxidative [corrected] stress in Alzheimer's disease. *Am J Pathol* **1992,** 140, 621-628.
3. Truscott, R. J. Age-related nuclear cataract-oxidation is the key. *Experimental Eye Research* **2005,** 80, 709-725.
4. Christen, Y. Oxidative stress and Alzheimer disease. *Am J Clin Nutr* **2000,** 71, 621S-629S.
5. Garner, B.; Roberg, K.; Qian, M.; Eaton, J. W.; Truscott, R. J. Distribution of ferritin and redox-active transition metals in normal and cataractous human lenses. *Experimental Eye Research* **2000,** 71, 599-607.
6. Dunaief, J. L.; Richa, C.; Franks, E. P.; Schultze, R. L.; Aleman, T. S.; Schenck, J. F.; Zimmerman, E. A.; Brooks, D. G. Macular degeneration in a patient with aceruloplasminemia, a disease associated with retinal iron overload. *Ophthalmology* **2005,** 112, 1062-1065.

7. Krishan, S.; Jansson, P. J.; Gutierrez, E.; Lane, D. J.; Richardson, D.; Sahni, S. Iron Metabolism and Autophagy: A Poorly Explored Relationship That Has Important Consequences for Health and Disease. *Nagoya J Med Sci* **2015,** 77, 1-6.

8. Ward, R. J.; Zucca, F. A.; Duyn, J. H.; Crichton, R. R.; Zecca, L. The role of iron in brain ageing and neurodegenerative disorders. *Lancet Neurol* **2014,** 13, 1045-1060.

9. Aust, S. D.; Morehouse, L. A.; Thomas, C. E. Role of metals in oxygen radical reactions. *J Free Radic Biol Med* **1985,** 1, 3-25.

10. Hernandez, R. B.; Farina, M.; Esposito, B. P.; Souza-Pinto, N. C.; Barbosa, F., Jr.; Sunol, C. Mechanisms of manganese-induced neurotoxicity in primary neuronal cultures: the role of manganese speciation and cell type. *Toxicol Sci* **2011,** 124, 414-423.

11. Quintanar, L. Manganese neurotoxicity: A bioinorganic chemist's perspective. *Inorganica Chimica Acta* **2008,** 361, 875–884.

12. Benedetto, A.; Au, C.; Aschner, M. Manganese-induced dopaminergic neurodegeneration: insights into mechanisms and genetics shared with Parkinson's disease. *Chem Rev* **2009,** 109, 4862-4884.

13. Yin, Z.; Aschner, J. L.; dos Santos, A. P.; Aschner, M. Mitochondrial-dependent manganese neurotoxicity in rat primary astrocyte cultures. *Brain Res* **2008,** 1203, 1-11.

14. Xie, H.; Hou, S.; Jiang, J.; Sekutowicz, M.; Kelly, J.; Bacskai, B. J. Rapid cell death is preceded by amyloid plaque-mediated oxidative stress. *Proc Natl Acad Sci U S A* **2013,** 110, 7904-7909.

15. Anderson, L. M. Cancer biology and hormesis: comments on Calabrese (2005). *Crit Rev Toxicol* **2005,** 35, 583-586.

16. Bruban, J.; Glotin, A. L.; Dinet, V.; Chalour, N.; Sennlaub, F.; Jonet, L.; An, N.; Faussat, A. M.; Mascarelli, F. Amyloid-beta(1-42) alters structure and function of retinal pigmented epithelial cells. *Aging Cell* **2009,** 8, 162-177.

17. Goldstein, L. E.; Muffat, J. A.; Cherny, R. A.; Moir, R. D.; Ericsson, M. H.; Huang, X.; Mavros, C.; Coccia, J. A.; Faget, K. Y.; Fitch, K. A.; Masters, C. L.; Tanzi, R. E.; Chylack, L. T., Jr.; Bush, A. I. Cytosolic beta-amyloid deposition and supranuclear cataracts in lenses from people with Alzheimer's disease. *Lancet* **2003,** 361, 1258-1265.

18. Lee, S.; Carson, K.; Rice-Ficht, A.; Good, T. Hsp20, a novel alpha-crystallin, prevents Abeta fibril formation and toxicity. *Protein Sci* **2005,** 14, 593-601.

19. Hardy, J. The amyloid hypothesis for Alzheimer's disease: a critical reappraisal. *J Neurochem* **2009,** 110, 1129-1134.

20. Citron, M. Alzheimer's disease: strategies for disease modification. *Nat Rev Drug Discov* **2010,** 9, 387-398.

21. Greenough, M. A.; Camakaris, J.; Bush, A. I. Metal dyshomeostasis and oxidative stress in Alzheimer's disease. *Neurochem Int* **2013,** 62, 540-555.

22. Bolognin, S.; Drago, D.; Messori, L.; Zatta, P. Chelation therapy for neurodegenerative diseases. *Med Res Rev* **2009,** 29, 547-570.

23. Adlard, P. A.; Parncutt, J.; Lal, V.; James, S.; Hare, D.; Doble, P.; Finkelstein, D. I.; Bush, A. I. Metal chaperones prevent zinc-mediated cognitive decline. *Neurobiol Dis* **2014**.

24. Schreurs, B. G. Cholesterol and copper affect learning and memory in the rabbit. *Int J Alzheimers Dis* **2013,** 2013, 518780.

25. Xiao, G.; Fan, Q.; Wang, X.; Zhou, B. Huntington disease arises from a combinatory toxicity of polyglutamine and copper binding. *Proc Natl Acad Sci U S A* **2013,** 110, 14995-5000.

26. Hogarth, P. Neurodegeneration with brain iron accumulation: diagnosis and management. *J Mov Disord* **2015,** 8, 1-13.

27. Cherny, R. A.; Atwood, C. S.; Xilinas, M. E.; Gray, D. N.; Jones, W. D.; McLean, C. A.; Barnham, K. J.; Volitakis, I.; Fraser, F. W.; Kim, Y.; Huang, X.; Goldstein, L. E.; Moir, R. D.; Lim, J. T.; Beyreuther, K.; Zheng, H.; Tanzi, R. E.; Masters, C. L.; Bush, A. I. Treatment with a copper-zinc chelator markedly and rapidly inhibits beta-amyloid accumulation in Alzheimer's disease transgenic mice. *Neuron* **2001,** 30, 665-676.

28. Adlard, P. A.; Cherny, R. A.; Finkelstein, D. I.; Gautier, E.; Robb, E.; Cortes, M.; Volitakis, I.; Liu, X.; Smith, J. P.; Perez, K.; Laughton, K.; Li, Q. X.; Charman, S. A.; Nicolazzo, J. A.; Wilkins, S.; Deleva, K.; Lynch, T.; Kok, G.; Ritchie, C. W.; Tanzi, R. E.; Cappai, R.; Masters, C. L.; Barnham, K. J.; Bush, A. I. Rapid restoration of cognition in Alzheimer's transgenic mice with 8-hydroxy quinoline analogs is associated with decreased interstitial Abeta. *Neuron* **2008,** 59, 43-55.

29. Faux, N. G.; Ritchie, C. W.; Gunn, A.; Rembach, A.; Tsatsanis, A.; Bedo, J.; Harrison, J.; Lannfelt, L.; Blennow, K.; Zetterberg, H.; Ingelsson, M.; Masters, C. L.; Tanzi, R. E.; Cummings, J. L.; Herd, C. M.; Bush, A. I. PBT2 rapidly improves cognition in Alzheimer's Disease: additional phase II analyses. *J Alzheimers Dis* **2010,** 20, 509-516.

30. Lannfelt, L.; Blennow, K.; Zetterberg, H.; Batsman, S.; Ames, D.; Harrison, J.; Masters, C. L.; Targum, S.; Bush, A. I.; Murdoch, R.; Wilson, J.; Ritchie, C. W. Safety, efficacy, and biomarker findings of PBT2 in targeting Abeta as a modifying therapy for Alzheimer's disease: a phase IIa, double-blind, randomised, placebo-controlled trial. *Lancet Neurol* **2008,** 7, 779-786.

31. Huntington Study Group Reach, H. D. I. Safety, tolerability, and efficacy of PBT2 in Huntington's disease: a phase 2, randomised, double-blind, placebo-controlled trial. *Lancet Neurol* **2015,** 14, 39-47.

32. Sampson, E. L.; Jenagaratnam, L.; McShane, R. Metal protein attenuating compounds for the treatment of Alzheimer's dementia. *Cochrane Database Syst Rev* **2012,** 5, CD005380.

33. Dumont, M.; Lin, M. T.; Beal, M. F. Mitochondria and antioxidant targeted therapeutic strategies for Alzheimer's disease. *J Alzheimers Dis* **2010,** 20 Suppl 2, S633-S643.

34. Rodríguez-Rodríguez, C.; Telpoukhovskaia, M.; Orvig, C. The art of building multifunctional metal-binding agents from basic molecular scaffolds for the potential application in neurodegenerative diseases. *Coordination Chemistry Reviews* **2012,** 256, 2308-2332.

35. Jin, H.; Randazzo, J.; Zhang, P.; Kador, P. F. Multifunctional antioxidants for the treatment of age-related diseases. *J Med Chem* **2010,** 53, 1117-1127.

36. Randazzo, J.; Zhang, P.; Makita, J.; Blessing, K.; Kador, P. F. Orally active multi-functional antioxidants delay cataract formation in streptozotocin (type 1) diabetic and gamma-irradiated rats. *PloS one* **2011,** 6, e18980.

37. Randazzo, J.; Zhang, Z.; Hoff, M.; Kawada, H.; Sachs, A.; Yuan, Y.; Haider, N.; Kador, P. Orally active multi-functional antioxidants are neuroprotective in a rat model of light-induced retinal damage. *PloS one* **2011,** 6, e21926.

38. Kawada, H.; Blessing, K.; Kiyota, T.; Woolman, T.; Winchester, L.; Kador, P. F. Effects of multifunctional antioxidants on mitochondrial dysfunction and amyloid-beta metal dyshomeostasis. *J Alzheimers Dis* **2015,** 44, 297-307.

39. Lipinski, C. A.; Lombardo, F.; Dominy, B. W.; Feeney, P. J. Experimental and computational approaches to estimate solubility and permeability in drug discovery and development settings. *Adv Drug Deliv Rev* **2001,** 46, 3-26.

40. Huang, C. Y. Determination of binding stoichiometry by the continuous variation method: the Job plot. *Methods Enzymol* **1982,** 87, 509-525.

41. Bradford, M. M. A rapid and sensitive method for the quantitation of microgram quantities of protein utilizing the principle of protein-dye binding. *Anal Biochem* **1976,** 72, 248-254.

TABLE OF CONTENTS GRAPHIC

Figure 1. Structures of the first generation of multifunctional antioxidants (MFAO-1s)

Figure 2. Structures of synthesized compounds in the MFAO-2 series. Shown are multifunctional compounds **2**, **4**, **6**, and **8;** mono-functional chelators (CHL), **1**, **3**, **5**, and **7**; monofunctional free radical scavengers (FRS), **10**, **12**, **14**, and **16**, and the non-functional parent compounds, **9**, **11**, **13**, and **15.**

Figure 3. Effect of compound exposure on cell viability of hNBs and RPE cells measured by the MTS viability assay. **A** illustrates the cell viability of RPEs after 2 h exposure to 1 mM of compounds **1-16**, clioquinol, or Trolox. **B** illustrates the cell viability of hNBs after similar exposure to compounds. The results represent the mean ± SEM, n = 4. Significant differences ($p < 0.05$), calculated by ANOVA, were compared to blank control.

Figure 4. MTS cell viability assay of hNBs and RPEs exposed with/without the presence of compounds to hydroxyl radicals generated via the Fenton reaction. **A** illustrates the cell viability of RPEs exposed for 2 h to 1 mM of Fenton reagent with/without the presence of 1 mM of compounds **1-16**, clioquinol, or Trolox. **B** illustrates the cell viability of similarly exposed hNBs. The results represent the mean ± SEM, n=4. Statistical significant differences, calculated by ANOVA, were as follows: * $p < 0.05$ versus control, # $p < 0.05$ versus clioquinol, and ł $p < 0.05$ versus Trolox.

Figure 5. Changes in GSH levels in cells exposed to hydroxyl radicals with/without the presence of compounds **1**-**16**, Trolox, or clioquinol. **B** illustrates GSH levels of RPEs exposed for 2 h with 1 mM of Fenton reagent with/without the presence of 1 mM of compounds **1-16**, clioquinol, or Trolox. **B** illustrates GSH levels of similarly exposed hNB cells. The results represent the mean ± SEM (n = 6). Significant differences, calculated by ANOVA, were as follows: * $p < 0.05$ versus control, # $p < 0.05$ versus clioquinol, and ł $p < 0.05$ versus Trolox.

Figure 6. Dose-dependent reduction of superoxide generated by xanthine oxidase and measured by MitoSOX staining in hNB and RPE cells. In **A** hNBs were pre-incubated with/without the presence of 1, 10, 100, 1000 μM compounds **2**, **4**, **9**, **11**, JHX-**4**, clioquinol or Trolox as well as SOD (25 μg/mL, approximately 100 μM) for 1 h and then exposed to xanthine oxidase (25 mU/mL) which can generate approximately 100 μM of superoxide for 1 h. **B** illustrates the results of similar experimental procedures of RPEs. The results represents mean ± SEM, n = 6.

Figure 7. Dose-dependent protection of cells against hydroxyl radicals measured with the LIVE/DEAD Viability Assay. **A** illustrates the results of hNB cells that were pre-incubated for 1 h with or without the presence of 1, 10, 100, 1000 μM of compounds **2**, **4**, **9**, **11**, JHX-**4**, clioquinol, or Trolox for 1h and exposed to 100 μM Fenton reagent for 2h. **B** illustrates the results of similar exposure of RPEs as above. The results represents mean ± SEM, n = 6.

Figure 8. Oral bioavailability of MFAOs in mice. Tissue levels of MFAOs measured in the brain (**A**), neural retina (**B**), and lens (**C**) of C57BL/6 mice fed chow containing

0.05% of each MFAO (80 mg/kg/day average dose) for 14 days. The results represent the mean ± SEM (n = 6-7). The present MFAO-2s achieved higher brain levels compared to the previously synthesized MFAO-1s (**A**) but failed to reach adequate levels in the lens (**C**). Similar neural retinal levels were observed with both MFAO-1s and MFAO-2s (**B**).

Table 1. Compound to metal ion ratio of select metal ions. The stoichiometry of the compound to metal complexes was obtained from the intersection of lines in Job's plots. The total concentration of the compound **1-8** and metal ion was 0.1 - 0.5 mM. * Non-intersecting lines on the Job Plot. Mean ± S.D.; n=3